1986

NMR studies of catalysts: phosphorous-31 and vanadium-51 in vanadium-phosphorous-oxygen selective oxidation catalysts and the selective averaging of the second order quadrupolar interaction in aluminosilicates

Russell Don Walker
Iowa State University

Walker, Russell Don

NMR STUDIES OF CATALYSTS: PHOSPHOROUS-31 AND VANADIUM-51 IN VANADIUM-PHOSPHOROUS-OXYGEN SELECTIVE OXIDATION CATALYSTS AND THE SELECTIVE AVERAGING OF THE SECOND ORDER QUADRUPOLAR INTERACTION IN ALUMINOSILICATES

Iowa State University PH.D. 1986

PLEASE NOTE:

In all cases this material has been filmed in the best possible way from the available copy. Problems encountered with this document have been identified here with a check mark __√__.

1. Glossy photographs or pages _____
2. Colored illustrations, paper or print _____
3. Photographs with dark background _____
4. Illustrations are poor copy _____
5. Pages with black marks, not original copy _____
6. Print shows through as there is text on both sides of page _____
7. Indistinct, broken or small print on several pages __√__
8. Print exceeds margin requirements _____
9. Tightly bound copy with print lost in spine _____
10. Computer printout pages with indistinct print _____
11. Page(s) _____ lacking when material received, and not available from school or author.
12. Page(s) _____ seem to be missing in numbering only as text follows.
13. Two pages numbered _____. Text follows.
14. Curling and wrinkled pages _____
15. Dissertation contains pages with print at a slant, filmed as received _____
16. Other _____

_____

_____

NMR studies of catalysts: Phosphorous-31 and vanadium-51 in vanadium-phosphorous-oxygen selective oxidation catalysts and the selective averaging of the second order quadrupolar interaction in aluminosilicates

by

Russell Don Walker

A Dissertation Submitted to the
Graduate Faculty in Partial Fulfillment of the
Requirements for the Degree of
DOCTOR OF PHILOSOPHY

Department: Chemistry
Major: Analytical Chemistry

Approved:

Signature was redacted for privacy.
In Charge of Major Work

Signature was redacted for privacy.
For the Major Department

Signature was redacted for privacy.
For the Graduate College

Iowa State University
Ames, Iowa

1986

TABLE OF CONTENTS

DEDICATION

To Mom and Dad, for their generous
and unflagging support and encouragement.

INTRODUCTION

Catalysis is a phenomenon of utmost importance in our technologically advanced way of life, and is fundamental even to the existence of life itself. Nature's most well-known catalysts, the enzymes of living systems, are indispensable to the function of even the simplest organisms. The enzymes are perhaps still the best standards of selectivity and efficiency against which the catalysts designed by man can be judged. To a large extent, the ability of technology to satisfy the demands of modern society for economical and useful products, particularly the ubiquitous products derived from oil, depends on the design of selective and active catalysts.

Many industrial catalysts have found wide use on a production scale even before the catalyst or its mechanism has become well-characterized. Extensive research effort continues in the expectation that new insight into the structure and mechanism of a catalyst will lead to improved versions of the catalyst. The work presented in this dissertation is part of such an effort. Vanadium-phosphorous-oxygen selective oxidation catalysts have found wide use in recent years but are still not well-understood. The first part of this dissertation attempts to provide chemical and structural details of these catalysts. Zeolites have proven to be extremely useful in oil refining processes, and the second part of this dissertation describes experiments conducted to facilitate the study of aluminum in zeolite structures.

PART ONE. PHOSPHOROUS-31 AND VANADIUM-51 IN VANADIUM-PHOSPHOROUS-OXYGEN SELECTIVE OXIDATION CATALYSTS

INTRODUCTION

The petrochemical industry relies on unsaturated hydrocarbons obtained from the oil refining process to produce derivative chemicals. An important derivative is maleic anhydride, which is used in the production of unsaturated polyester resins, lubricating oil additives, agricultural chemicals and copolymers, and whose consumption is growing at the rate of about 8% annually (1). For many years, maleic anhydride was produced commercially by the oxidation of benzene. However, in recent years, considerable attention has been focused on the production of maleic anhydride by the oxidation of C_4 fractions, mainly n-butane and 1-butene, a process which may prove to be more economically desirable.

Since production of maleic anhydride for commercial sale began in 1933, the dominant process has been the oxidation of benzene vapor (2). The catalysts presently used contain V_2O_5 and MoO_3, with As, Co, Na, Li, TiO_3, WO_3 or P_2O_5 added to enhance yield, and are supported on alumina, silica or carborundum. In recent years, high oil prices have made benzene increasingly expensive, and coupled with the increasing demand for aromatics in unleaded gasoline, have made the use of benzene as a feedstock less economically desirable (3). In addition, tight controls on benzene emissions from maleic anhydride plants have been implemented by the Environmental Protection Agency.

The low cost of butane and recent development of improved catalysts for the oxidation of butane to maleic anhydride have made the use of butane as a feedstock more desirable than benzene. In the 1970s, more than 70 patents related to the oxidation of butane to maleic anhydride were issued (2). The catalysts reported most often were vanadium-phosphorous oxides, either alone or mixed with activating modifiers such as Fe, Cr, Ti, Co, Ni, Zr, Zn, Mo or Cu. Although the oxidation of butane contributed to only 15% of all maleic anhydride produced in 1979 (2), the process based on the oxidation of benzene has been displaced to the extent that for 1984, 85% of production was expected to be from the oxidation of C_4 fractions (3).

The oxidation of butane to maleic anhydride is an example of a selective oxidation process. Catalysts for selective oxidation must provide only enough oxygen to the reactant to allow the formation of the desired product without any further oxidation to CO or CO_2. The selective oxidation process is considered to be a two stage redox reaction that proceeds according to the Mars and van Krevelen mechanism (4). In the first stage, the reactant is adsorbed then oxidized to product by the catalyst, and the product is desorbed. In the second stage, the reduced catalyst is reoxidized by oxygen dissociatively adsorbed from the feed stream. However, the degree to which oxygen in the bulk of the catalyst participates in what could conceivably be strictly a surface process is an open question (5).

Studies of the selective oxidation of butane and butene to maleic anhydride over vanadium-phosphorous oxides have focused on the unsupported mixed oxide without any modifiers. It is generally agreed that for such a catalyst to be selective the ratio of phosphorous to vanadium must be close to one, but the exact effect of the P/V atomic ratio depends on the method of synthesis, including the reducing medium (organic or aqueous) (3,6), and calcination temperature, duration and atmosphere (7-9). Several different phases have been identified in fresh and used catalysts for a range of preparations and values of P/V (3). These phases include α- and β-$VOPO_4$, in which most vanadium is V(V), and $(VO)_2P_2O_7$ and the B-, B'-, β- and β^*-phases, where most vanadium is V(IV). The B-, β- and $(VO)_2P_2O_7$ phases have very similar principal d spacings in their x-ray diffraction patterns. The oxidation states of vanadium involved in the catalytic reaction are considered to be V(V) and V(IV). Some workers have proposed a role for V(III) also (6,8). It is generally believed that vanadyl phosphate (β-$VOPO_4$, in which vanadium is nominally V(V)) and vanadyl pyrophosphate ($(VO)_2P_2O_7$, in which vanadium is nominally V(IV)) play a role in the process.

In an often quoted work, Bordes and Courtine (10) reported that in spent catalysts with $0.5 < P/V < 1.8$, both $VOPO_4$ and $(VO)_2P_2O_7$ were present and necessary for a substantial selectivity in the oxidation of butene to maleic anhydride. They proposed that microdomains of $VOPO_4$ coexist within lar-

ger domains of $(VO)_2P_2O_7$, and that the active and selective sites are located near the boundary between the two domains.

Further studies focused on the synthesis and interconvertibility of different forms of $VOPO_4$ and $(VO)_2P_2O_7$. γ-$(VO)_2P_2O_7$ was found to be a mixed valence compound that acts as a catalyst by itself without structural change; pairs of VO_6 octahedra at the (010) surface were considered to be the active sites (11). Synthesis conditions governed the morphology of the precursor, and, through topotactic dehydration, the crystal face exposed in $(VO)_2P_2O_7$ (12). The gamma form of $(VO)_2P_2O_7$ was active and selective in the oxidation of butane to maleic anhydride. The oxidation of butene involved the β-$(VO)_2P_2O_7/\beta$-$VOPO_4$ system and the active site was believed to be a single VO_6 octahedron at the interface between the two compounds (12,13).

Cavani et al. (14-16) found that for preparations with $0.95 < P/V < 1.2$, only a single-phase nonstoichiometric pyrophosphate of V(IV), called the B phase, was obtained. Without any apparent modification of structure, the B phase maintained high concentrations of vanadium oxidation states other than V(IV) (14). In one case, chemical analysis showed that about 20% of the vanadium was present as V(V) (15). For B phases prepared with $P/V < 1$, the rate of formation of V(V) during reaction was higher than when $P/V > 1$, and the distribution of V(V) determined the relative rates of maleic anhydride formation and decomposition to carbon oxides. In B phases with $P/V > 1$, the excess phosphorous stabilized V(IV)

and resulted in decreased activity and selectivity of butane oxidation to maleic anhydride.

Recent work by Pepera et al. (5) focused on the role of the catalyst surface. β-$(VO)_2P_2O_7$ catalyzed the oxidation of butane through the redox reaction of its surface but with kinetics characteristic of the bulk. Surface V(IV) activated O-O and C-H bonds while surface V(V) converted the activated butane to products. The confinement of the redox process to the surface was attributed to the stability of V(IV) in the bulk.

The effect of P/V on the composition and behavior of catalysts with $0.94 < P/V < 1.07$. was studied by Hodnett et al. (7,17,18). An excess of phosphorous ($P/V > 1$) inhibited both the oxidation and reduction of the bulk, but had little effect on the reactivity of near-surface layers. The primary interaction between n-butane and catalyst was associated with V(V) on the surface (17). The highest selectivity coincided with the P/V that resulted in the highest concentration of V(IV) (18). The effect of a deficiency of phosphorous was to make available lattice oxygen from the bulk so that the intermediates could react nonselectively with this excess of oxygen. For $P/V > 0.97$, both surface P/V and surface V(V)/V(IV) were invariant. The catalytic process caused a small increase in the average oxidation state of vanadium.

Centi and Trifiro (19) considered the relative participation of oxygen from the feed stream and from the catalyst and found that without the presence of O_2 gas, the B phase

catalyst forms only the intermediate butadiene from 1-butene. In the presence of O_2 gas, α-$VOPO_4$ caused total oxidation of 1-butene to CO and CO_2.

The purpose of this work is to use the methods of magnetic resonance, and in particular nuclear magnetic resonance, to characterize the vanadium-phosphorous oxide (VPO) catalysts for the selective oxidation of butane and butene to maleic anhydride. The primary goal is to provide information on the oxidation states of vanadium in the catalysts. A secondary goal is to provide some insight into the catalyst structures, in particular any structural changes induced by the catalytic process.

The utility of nuclear magnetic resonance in this investigation lies in its sensitivity to the electronic environment surrounding the phosphorous and vanadium nuclei. The frequency and lineshape of the NMR signal is dependent on both the chemical shift, which is sensitive to the electronic environment, and the proximity of paramagnetic centers. The character of the vanadium signal is especially sensitive to distortions in the symmetry of the ligands around the vanadium atoms due to the electric quadrupole moment of the vanadium nucleus. Electron paramagnetic resonance is also useful because of the influence of coordination symmetry on lineshape and its sensitivity to the concentration of paramagnetic centers. While EPR has been employed in a number of studies of VPO systems, it is believed that this work is the first application of NMR to the study of VPO catalysts.

The work reported here was performed in collaboration with Thomas P. Moser and Robert W. Wenig, whose research was directed by Dr. Glenn L. Schrader, Department of Chemical Engineering, Iowa State University. The catalysts studied were the model compounds β-$VOPO_4$ and $(VO)_2P_2O_7$, and the precatalysts and B phase catalysts with P/V = 0.9, 1.0 and 1.1. The precatalyst is the solid product formed from the synthesis suspension, and the B phase is obtained by the calcination in air of the precatalyst. Details of the preparation of the model compounds (20), precatalysts and B phase catalysts (21) are given elsewhere.

NMR OF PARAMAGNETIC COMPOUNDS

The presence of an unpaired electron in a paramagnetic compound can have two effects on the NMR spectrum of a nearby nucleus. In one case, the signal is unobservable, while in the other case, the absorption line is broadened and possibly shifted from the frequency that it would have in an analagous diamagnetic compound. Through motion, the large magnetic moment of an unpaired electron can produce a very intense fluctuating magnetic field. If the frequency components of the motion are large at the frequency corresponding to A_H, the electron spin - nuclear spin hyperfine coupling constant, then the nuclear relaxation will be very efficient, leading to a short T_1 and a resonance so broad as to be unobservable (22).

However, if the electronic relaxation time T_{1e} is so short that $1/T_{1e} >> A_H$, then the nucleus will interact with only a population-weighted average of the two electron spin states, thus decreasing the efficiency of the relaxation. In this case, the nuclear T_1 is not so severely shortened, and the NMR absorption line may be narrow enough to be observed, though usually not as narrow as it would be in an analogous diamagnetic compound (23). At convenient temperatures, the population-weighted average of the electron spin states differs significantly from zero, and gives rise to two interactions that shift the NMR absorption frequency, the Fermi contact interaction and the dipolar interaction (24).

The Fermi contact coupling is a result of the direct interaction of the nuclear spin and electron spin, and is given by $A_F\vec{I}\cdot\vec{S}$, where A_F is the coupling constant. This interaction produces the contact, or scalar shift, which can be described by (25)

$$\Delta H/H_o = -[A_N g_e^2 \beta_e^2 S(S+1)] \; / \; (g_N \beta_N 3kT),$$

where $A_N = (8\pi/3) g_N \beta_N |\psi(0)_N|^2$, g_e, g_N and β_e, β_N are the g factors and magnetons for the electron and nucleus and S is the spin angular momentum quantum number for the electron spin system. The origin of the shift is the magnetic field that arises from unpaired electron density at the nucleus, $|\psi(0)_N|^2$. Thus the nuclear resonance will only experience a contact shift if the unpaired electron resides in an orbital (associated with the nucleus observed) having s character.

The second kind of shift comes from the local magnetic field created by the unpaired electron spin through the magnetic dipole interaction. The dipolar, or pseudocontact shift, is usually described by (25)

$$\frac{\Delta H}{H_o} = \frac{-\beta_e^2 S(S+1)}{9kT|\vec{r}|^3} \left[(3\cos^2\theta - 1)\left(g_{zz}^2 - \tfrac{1}{2}g_{xx}^2 - \tfrac{1}{2}g_{yy}^2\right) + \tfrac{3}{2}\sin^2\theta\cos 2\phi\left(g_{xx}^2 - g_{yy}^2\right) \right]$$

where $\vec{r}$ is the vector between the nucleus and electron, and θ and ϕ are the Euler angles associated with $\vec{r}$ and the principal axis system of the electron g tensor.

The expressions given for the contact and dipolar shifts are based on several assumptions (24-26). First, it is assumed that the system has only one thermally populated

energy level in the absence of a magnetic field, and second, that there is at most only a first order contribution of orbital coupling to the magnetic moment of the complex, which is caused by the spin-orbit mixing of the ground level with nonpopulated excited states. For systems with a T_2 ground term, such as the V(IV) of interest in this study, both of these assumptions are violated. A third assumption is that zero field splitting can be ignored. In the case of V(III), there is almost definitely a large zero-field splitting (27). Finally, for the dipolar shift, it was assumed that the unpaired electron was sufficiently distant from the nucleus that it could be treated as a point dipole.

Kurland and McGarvey derived more general expressions for the contact and dipolar shifts (26). In their perturbation approach, the Hamiltonians for the Fermi contact, magnetic dipolar and nuclear spin - electron orbital interactions act on eigenstates describing the system in the absence of a magnetic field. Of particular interest is the separation of the dipolar shift into two parts, one based on the interaction of unpaired electron spin in a ligand orbital with a ligand nucleus, and the other on the interaction of spin in a metal orbital with a ligand nucleus. The latter contribution is given by

$$\frac{\Delta H}{H_o} = (2|\vec{R}|^3)^{-1} [(1-3\cos^2\Omega)(\chi_{zz} - \bar{\chi}) + \sin^2\Omega\cos 2\phi(\chi_{yy} - \chi_{xx})]$$

where χ_{ii} are the principal components of the magnetic susceptibility tensor, $\vec{R}$ joins the metal and ligand nuclei

and Ω and ϕ are the Euler angles relating $\vec{R}$ to the principal axis system of the susceptibility tensor. When there is unpaired spin in the orbitals belonging to the nucleus of interest, R^{-3} is replaced by $\langle r^{-3} \rangle$, the average over the orbital.

In VPO catalysts, vanadium occurs as V(V), V(IV) and V(III). Both reduced states are paramagnetic, having the $3d^1$ and $3d^2$ configurations, respectively. It is expected that the presence of either of these two paramagnetic states will have an effect on both the ^{31}P and ^{51}V NMR spectra through relaxation effects and the dipolar shift. The use of the above expressions for the paramagnetic shift in a strictly quantitative fashion is outside the scope of this study.

NMR OF PHOSPHOROUS-31

General Considerations

Three properties of the phosphorous-31 nucleus make its study by nuclear magnetic resonance particularly attractive. The natural abundance of the ^{31}P nucleus is 100%, which in conjunction with the relatively high magnetogyric ratio (γ) of 1.72 kHz/gauss gives ^{31}P a favorable sensitivity. The γ of ^{31}P is not so great, however, that homonuclear dipolar interactions in solids are as troublesome as they are for ^{1}H. In the VPO compounds studied here, phosphorous is believed to reside only in PO_4 tetrahedra, so pairs of ^{31}P are unlikely to be closer than about 3 A, which implies a dipolar broadening of about 5 kHz. The spin angular momentum quantum number I for ^{31}P is 1/2, so that ^{31}P nuclei are not subject to the quadrupole interaction.

Although the quadrupolar interaction is often informative, the nonquadrupolar nature of ^{31}P is advantageous in the study of VPO catalysts because the interaction of ^{31}P nuclei with unpaired electrons is left as the most severe line broadening effect. For ^{51}V, which has an electric quadrupole moment, the distinction between quadrupolar and paramagnetic broadening is not readily made. Therefore the presence of ^{31}P enhances the possibility of detecting the effects of unpaired electrons in the VPO catalysts using NMR.

Chemical shifts for phosphorous in diamagnetic compounds range from -250 ppm (downfield) to +380 ppm (upfield) rela-

tive to ^{31}P in H_3PO_4, but the shifts for PO_4 groups in inorganic orthophosphates and condensed phosphates span a more narrow range, from -10 ppm to +50 ppm (28). The isotropic shift has been shown to depend on whether the PO_4 group is an isolated unit or an end, middle or branching unit in a chain or cage (29). The shift of isolated PO_4 units is usually -10 to +15 ppm, of end PO_4 units is -3 to +21 ppm, of middle units is +18 to +21 ppm and of branching units is +32 to +46 ppm.

The chemical shift anisotropies are more characteristic of the different types of condensed PO_4 group than the isotropic shifts. With the principal components of the chemical shift tensor defined such that $\sigma_{11} < \sigma_{22} < \sigma_{33}$, the value of $\sigma_{33} - \sigma_{22}$ for end groups is between 0 and 35 ppm, for middle groups is 135 to 225 ppm and for branching groups is 230 to 295 ppm (29).

In the VPO catalysts, ^{31}P is found in isolated PO_4 units and pyrophosphate PO_4 end units. In K_3PO_4, isolated PO_4 units have a shift of -10 ppm and no anisotropy (30), but in more complex compounds, such as $Na_8HW_9PO_{34}\cdot xH_2O$ or $KAs(PO_4)_2$, have isotropic shifts farther upfield and anisotropies (sometimes axially symmetric) between 18 and 180 ppm (31). Of the pyrophosphates $K_4P_2O_7$, $Na_4P_2O_7$ and α-$Ca_2P_2O_7$, PO_4 units in the first two have isotropic shifts between -2 and +1 ppm and axially symmetric anisotropies of ~120 ppm with $\sigma_\perp$ upfield; the last has a shift of +19 ppm and shielding components -45, +38 and +66 ppm (29).

Experimental Procedure

The ^{31}P NMR experiments were performed at a resonant frequency of 89.010 MHz. A detailed description of the spectrometer can be found elsewhere (32). A probe with a Q of ~180 was used, and 90° pulse lengths were ~1.5 μsec. Single phase detection and a 500 kHz low pass filter were used. Probe and filter had a combined ringdown time of ~25 μsec. The transient recorder was triggered 25 μsec after the 90° pulse and the transient was digitized at a rate of 5 MHz.

Typically about 8,000 free induction decays were coherently accumulated. Most samples had a T_1 of about 1 second, so a recycle time of 1 second was used to optimize the signal to noise ratio with respect to accumulation time (33). After a linear tapering of the later part of the transient, where only noise was evident, an 8K fast Fourier transform was performed. In spectra where widely separated peaks appeared, first order phase correction gave unsatisfactory results, so zero order correction was applied to each region of the spectrum independently.

The ^{31}P shifts are reported relative to ^{31}P in 85% H_3PO_4 using the σ convention, in which negative numbers indicate downfield (deshielded) shifts. Because of the extent to which H_3PO_4 detuned the NMR probe, trimethyl phosphate liquid was routinely used as a shift reference. The shifts relative to trimethyl phosphate were then adjusted to be relative to H_3PO_4 by subtracting 2.4 ppm (28).

Results

The ^{31}P NMR spectrum of the model compound vandayl phosphate, β-$VOPO_4$, is shown in Figure 1a. A single symmetric peak appears at +2 ppm, with full width at half maximum (FWHM) of 5 kHz. The four P-O bond lengths in the PO_4 units of this compound have been reported to fall within the range 1.52 to 1.54 A (34), so the symmetry of this peak is reasonable and the linewidth can be ascribed to dipolar interactions. The position and shape of the peak is consistent with results reported for other orthophosphates (31).

After exposure of β-$VOPO_4$ to a stream of 1.5% n-butane in air at 450°C. for 18 hours, the peak shifts slightly upfield to +12 ppm while the width and shape remain unchanged (Figure 1b). However, after a similar treatment with 1.5% 1-butene in air, the peak shifts to +87 ppm and becomes much weaker (as evidenced by the decrease in signal-to-noise ratio) and broader, with FWHM 20 kHz (Figure 1c). The vanadium in vanadyl phosphate is nominally V(V), but during exposure to butene a significant amount of V(V) could be reduced to V(IV) (35). Presumably the shift relative to the untreated compound is a dipolar shift due to paramagnetic V(IV), while the loss of intensity and increase in linewidth of the remaining signal is a result of rapid relaxation induced by V(IV).

The ^{31}P spectrum of the model compound vanadyl pyrophosphate, $(VO)_2P_2O_7$, is shown in Figure 2a. The low signal intensity is taken as an indication that a large number of the phosphorous nuclei are invisible due to extreme broadening

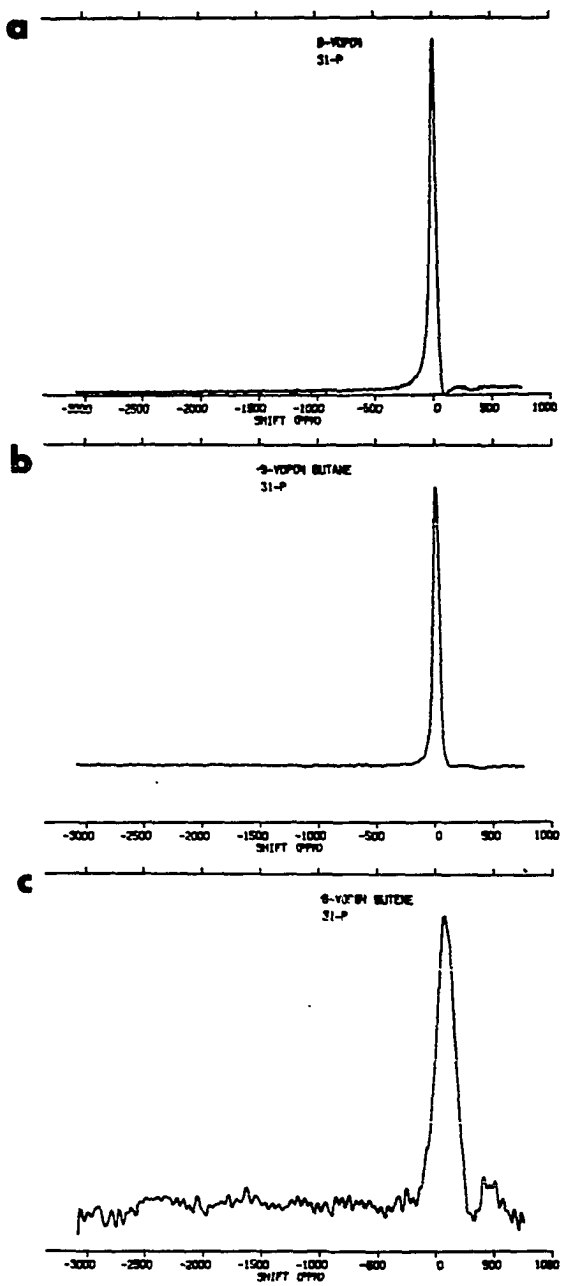

Figure 1. ^{31}P NMR spectra of β-$VOPO_4$ a) untreated, b) after butane treatment, and c) after butene treatment.

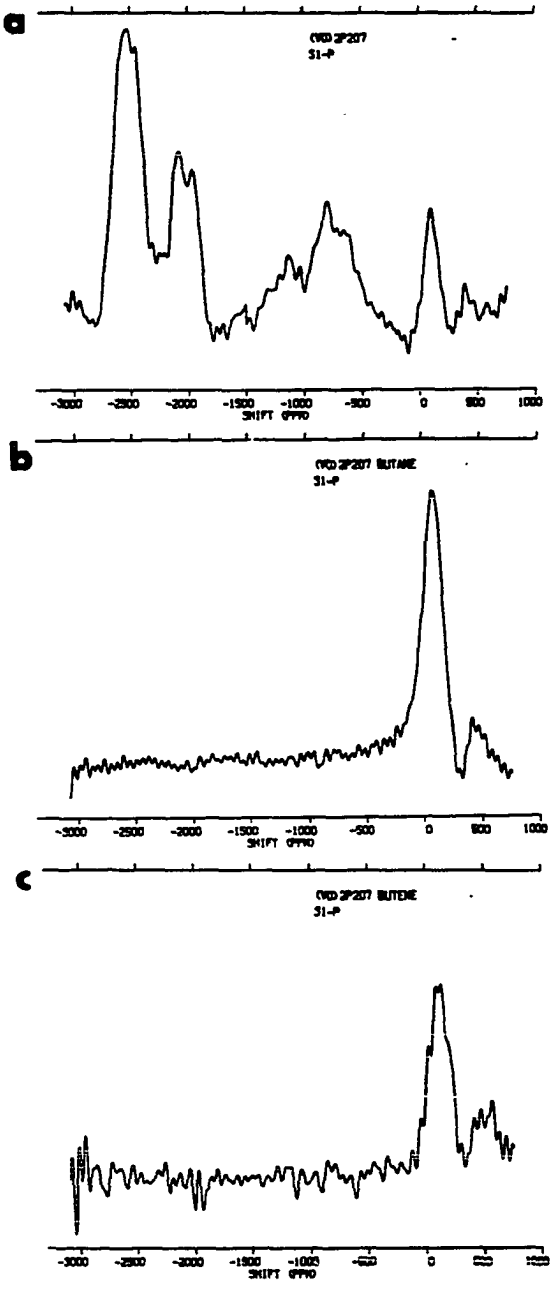

Figure 2. ^{31}P NMR spectra of $(VO)_2P_2O_7$ a) untreated, b) after butane treatment, and c) after butene treatment.

caused by the proximity of unpaired electron spin. Since the vanadium in this model compound is nominally all V(IV), this explanation seems reasonable.

An idealized structure of vanadyl pyrophosphate is shown in Figure 3. Double chains of VO_6 pseudooctahedra project from the plane of the diagram by sharing axial vertices through V=O-V bonding (36). Each phosphorous atom shares three oxygens with vanadium atoms in three different chains, and the P-O-P pyrophosphate bonds further connect the layers. In consideration of the structure, it is difficult to rationalize the presence of four different peaks in the spectrum. All but the peak at ~0 ppm are tentatively attributed to phosphorous shifted by the dipolar interaction, but the structure seems to imply only a single kind of phosphorous.

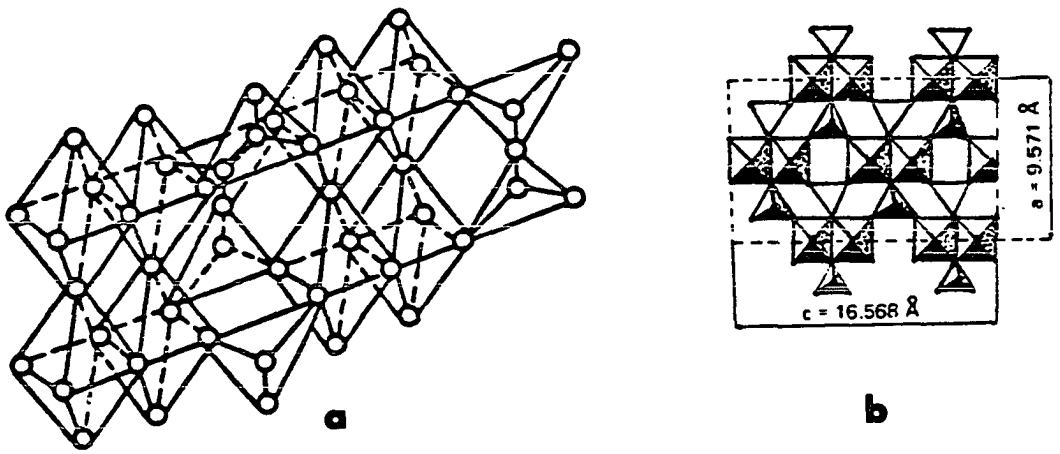

Figure 3. The idealized structure of $(VO)_2P_2O_7$ in a a) three-dimensional representation (37), and a b) projection onto the ac-plane (13).

Perhaps the ^{31}P peaks observed come from phosphorous near crystal defects that produce V(V). The distinct peaks could then be caused by different phosphorous sites with progressively less interaction with V(IV) in the bulk.

After exposure to either butane or butene (1.5% in air at 450°C. for 18 hours), the spectrum of $(VO)_2P_2O_7$ resembles the spectrum of β-$VOPO_4$ after exposure to butene (Figures 2b,c). The shift of the lone peak is +101 ppm and the width is 17 kHz; the peak from butene-treated $(VO)_2P_2O_7$ is less intense than the peak from butane-treated $(VO)_2P_2O_7$. The disappearance of the downfield dipolar shifted peaks after hydrocarbon treatment may be due to broadening caused by nearby unpaired electron spin. Even before exposure to hydrocarbons, the vanadium in $(VO)_2P_2O_7$ is nominally V(IV); the extent of reduction is expected to increase during treatment with butane or butene.

In the spectrum of the precatalysts with P/V = 0.9, 1.0 and 1.1, there is a peak at ~-1690 ppm, FWHM 24 kHz, and a peak at +13 ppm, FWHM 10 kHz (Figures 4a-c). As in the case of $(VO)_2P_2O_7$, the downfield peak is attributed to phosphorous shifted through the dipolar interaction with nearby unpaired electron spin. The precatalysts are in a highly reduced state and the presence of paramagnetic V(IV) is thus expected (38). As P/V increases, the area of the peak at ~-1690 ppm (relative to the total area of both peaks) decreases from 89% to 85% to 67%.

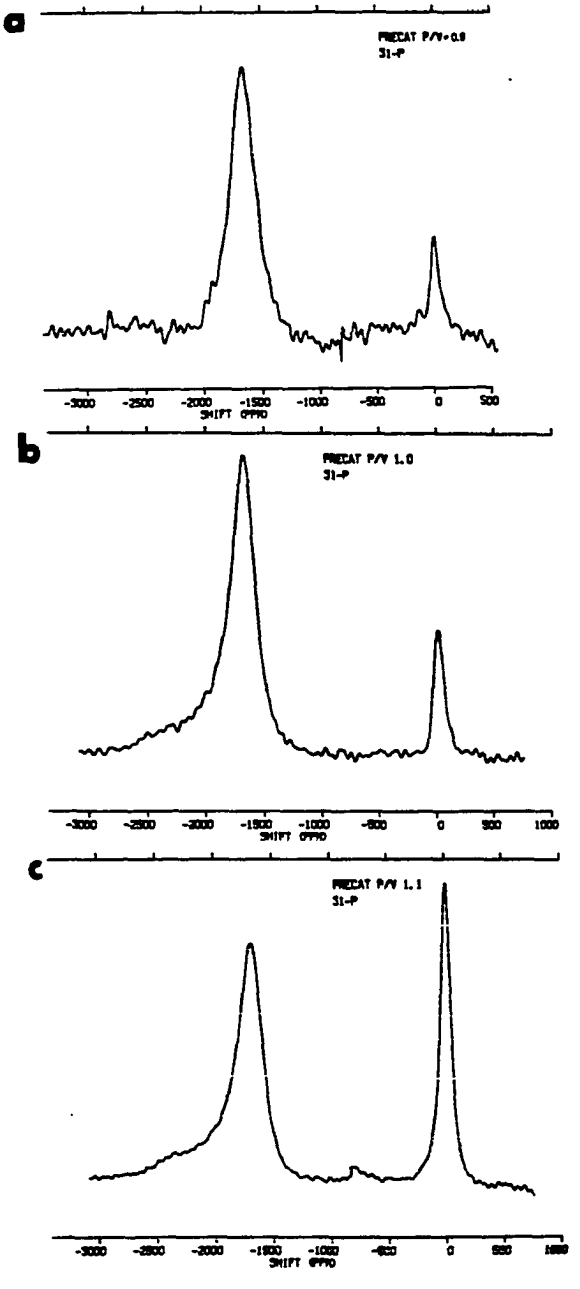

Figure 4. ^{31}P NMR spectra of a) precatalyst P/V = 0.9, b) precatalyst P/V = 1.0, and c) precatalyst P/V = 1.1.

An opposite trend in areas is evident in the spectra of the B phase catalysts. For B phase 0.9, only the peak at ~0 ppm is observed (Figure 5a). The dipolar shifted peak at ~-1690 ppm appears in the spectrum of B phase 1.0 and is only 12% of the total signal (Figure 5b), while in the spectrum of B phase 1.1, the dipolar shifted peak has grown to 75% of the total signal (Figure 5c).

After exposure to n-butane (identical to the treatment described above for the model compounds), the B phase 0.9 spectrum was unchanged, except for perhaps a decrease in intensity of the lone peak. The exposure to n-butane of B phases 1.0 and 1.1 removed both peaks. The complete absence of any ^{31}P NMR signal suggests that there is a large concentration of unpaired electron spin which is causing extreme line broadening for the phosphorous nuclei. This explanation is consistent with the expected reduction of the catalysts during treatment with n-butane (38).

The results of the ^{31}P NMR experiments are summarized in Table 1. It is noteworthy that none of the spectra exhibited any ^{31}P chemical shift anisotropy, and an important source of structural information is thus lost. Apparently the effects of unpaired electron spin mask any effects of chemical shift anisotropy.

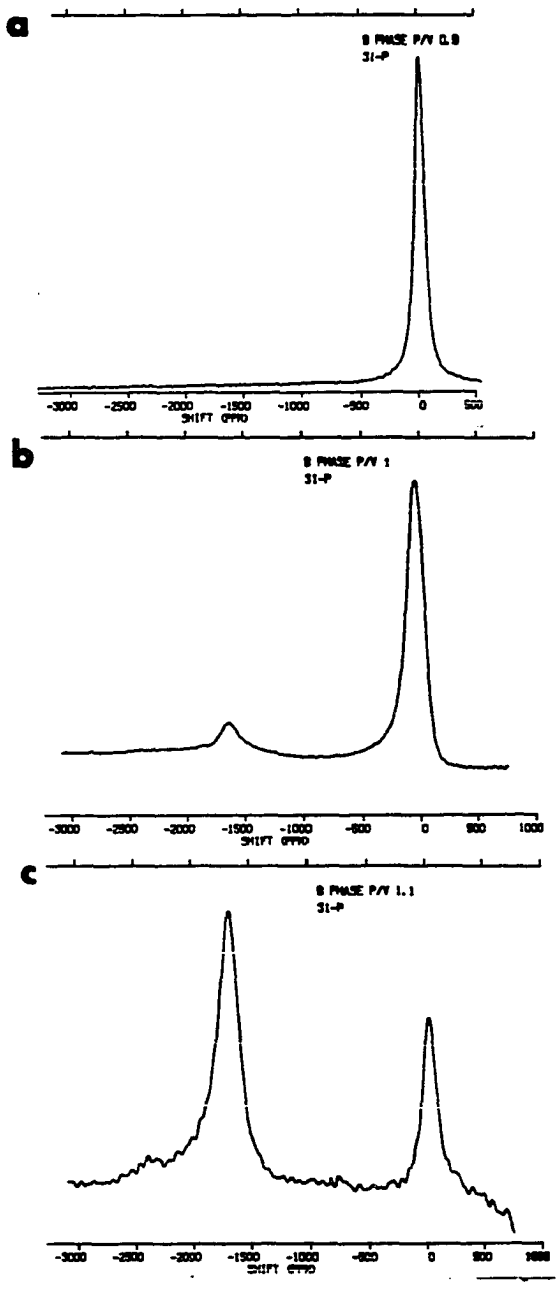

Figure 5. ^{31}P NMR spectra of untreated B phase catalysts with a) P/V = 0.9, b) P/V =1.0, and c) P/V = 1.1.

Table 1. ^{31}P NMR Results for VPO Catalysts

	shift in ppm (FWHM)[a]	
β-$VOPO_4$		
untreated	+2 (5 kHz)	
butane-treated	+12 (5 kHz)	
butene-treated	+87 (16 kHz)	
$(VO)_2P_2O_7$		
untreated	+93 (11 kHz),	-800 (32 khz),
	-2000 (21 kHz),	-2500 (21 kHz)
butane-treated	+101 (16 kHz)	
butene-treated	+101 (17 kHz)	
precatalysts		
P/V = 0.9	+13 (10 kHz),	-1710 (24 kHz)
P/V = 1.0	+13 (10 kHz),	-1690 (24 kHz)
P/V = 1.1	+13 (10 kHz),	-1680 (24 kHz)
B phase catalysts		
P/V = 0.9		
untreated	+18 (11 kHz)	
butane-treated	+15 (11 kHz)	
P/V = 1.0		
untreated	-36 (16 kHz),	-1680 (24 kHz)
butane-treated	no signal	
P/V = 1.1		
untreated	+29 (13 kHz),	-1670 (24 kHz)
butane-treated	no signal	

[a]Shifts are in ppm relative to ^{31}P in 85% H_3PO_4 using the σ convention.

NMR OF VANADIUM-51

General Considerations

Vanadium-51 is another nucleus whose study by nuclear magnetic resonance is appealing. Its natural abundance of 100% and fairly high magnetogyric ratio (γ) of 1.12 kHz/gauss give ^{51}V a favorable sensitivity. The γ of ^{51}V is low enough that at V-V internuclear distances likely to be found in this study (2.6 A for edge-shared VO_6 octahedra), the homonuclear dipolar broadening is only 3 kHz. Unlike ^{31}P, ^{51}V is an $I = 7/2$ nucleus and is subject to the quadrupolar interaction, which is a result of coupling between the electric quadrupole moment of the nucleus and the electric field gradient (due to the surrounding electronic environment) at the nucleus. The value of the electric quadrupole moment of ^{51}V is a matter of dispute, being reported as -0.05, +0.05, +0.21 and $+0.3 \times 10^{-28}$ m^2 (39). In any case, the quadrupole moment is small enough that in most samples the quadrupole broadening will not be so severe that the signal will be broadened into the baseline.

In the presence of an electric field gradient, the NMR signal from a nucleus with $I = 7/2$ is split into seven peaks. The most intense peak remains at about the frequency at which the nucleus would resonate in the absence of a quadrupolar interaction and it is this peak that is routinely observed. (Details of the quadrupole interaction between an electric field gradient and a nucleus with $I > 1/2$ are discussed in

Part Two of this thesis.) If the sample is a powder or amorphous, then the NMR spectrum is a distinctive powder pattern (Figure 6). The splitting between the innermost divergences in the first order powder pattern is a convenient measure of ν_Q, which for I = 7/2 and an axially symmetric electric field gradient ($\eta = 0$) is equal to $e^2qQ/14h$. The central peak also has a distinctive powder pattern (Figure 6). For I = 7/2 and $\eta = 0$, the splitting between the divergences in this pattern is given by $\Delta\nu = (125/48)(\nu_Q^2/\nu_o)$, and the shift in the center of gravity of the powder pattern from the unperturbed frequency is given by $\nu_o - \nu_{cg} = \nu_Q^2/2\nu_o$. In the case where there is a distribution in ν_Q throughout the sample, the satellite peaks occur over a range of frequencies and the

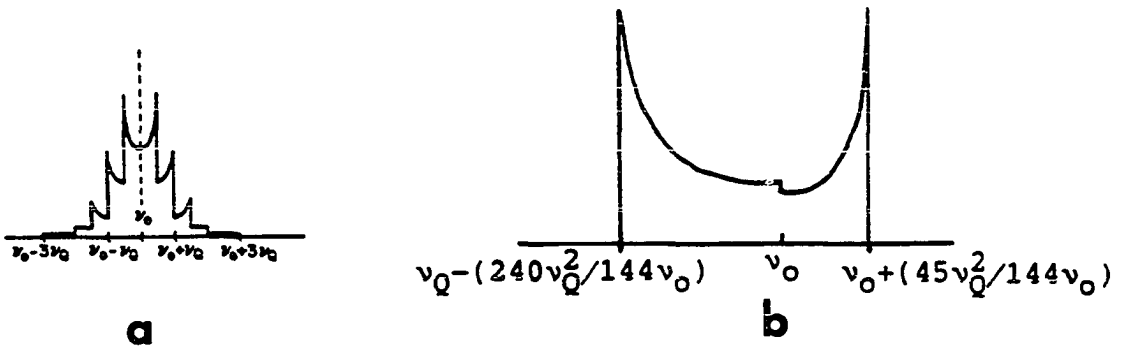

Figure 6. Powder patterns for a nucleus with I = 7/2 in an axially symmetric electric field gradient, showing the a) first order effect of the quadrupolar interaction, and b) second order effect on the central transition.

divergences in the powder pattern become less distinct, often to the point of invisibility. The same effect can similarly alter the appearance of the central transition powder pattern.

For inorganic solids with vanadium in VO_4 tetrahedra, the quadrupole coupling (e^2qQ/h) ranges from 0.5 to 6.8 MHz and the asymmetry parameter η ranges from 0 to 0.8 (39). Vanadium in the VO_6 pseudooctahedra of V_2O_5 has a quadrupole coupling of 800 kHz and an asymmetry parameter of about zero (40,41).

Chemical shifts of ^{51}V in diamagnetic compounds span a range of ~2500 ppm (42). Values for the isotropic shift of V(V) in VO_4 groups have been reported from +250 ppm (upfield) to -125 ppm (downfield) relative to aqueous KVO_3 (39). In moderate to strong magnetic fields, it is common for chemical shift anisotropy to dominate the shape of the central peak in powders. For VO_4 groups, the range of anisotropies reported is from 80 to 560 ppm, and most show no axial symmetry (39). For VO_6 groups in V_2O_5, the chemical shift anisotropy has been reported as $\sigma_{\perp} = +200$ ppm and $\sigma_{\parallel} = -350$ ppm (40), and as $\sigma_{xx} = +180$ ppm, $\sigma_{yy} = -650$ ppm and $\sigma_{zz} = +300$ ppm (41).

Experimental Procedure

The NMR experiments on ^{51}V were performed at 57.710 MHz on a spectrometer described elsewhere (32). Pulse length considerations are discussed in Part Two of this thesis.

Although at least some of the ^{51}V detected may have been excited nonselectively, 22.5° pulse lengths (relative to an aqueous solution of vanadium) were used as a compromise between excitation bandwidth and signal intensity. Using a probe with a Q of ~30, the pulse lengths for a flip angle of 22.5° were ~1 μsec. Single phase detection and a 500 kHz low pass filter were used. The combined ringdown time due to probe and filter was ~6 μsec. The transient recorder was triggered 7 μsec after the 22.5° pulse, and a digitization rate of 5 MHz was used.

Typically 32,000 free induction decays were coherently accumulated. A recycle time of 0.1 sec was used and was at least five times as great as T_1 for the samples. The data were treated as described for the ^{31}P NMR experiments, except that a single zero order phase correction was applied to the entire spectrum.

The ^{51}V chemical shifts are reported relative to an aqueous solution of NH_4VO_3 using the σ convention. An aqueous solution of aluminum was routinely used as a shift reference; the shifts relative to $Al(H_2O)_6^{3+}$ were adjusted to be relative to VO_3^- by subtracting 8810 ppm. Since the Q of the probe did not vary between the resonant frequencies of ^{51}V in VO_3^- and ^{27}Al in $Al(H_2O)_6^{3+}$, the aluminum solution was used to adjust pulse lengths.

Results

The results of the ^{51}V NMR experiments are summarized in Table 2, and the spectra are shown in Figures 8,10,11. The spectra show features in at least one of three chemical shift ranges (-150 to -1000 ppm, +150 to +260 ppm or +600 to +1200 ppm) or show no signal at all. The complete absence of signal can be attributed to a wide distribution of very large quadrupole couplings, or to extreme broadening induced by unpaired electrons.

Before reviewing the spectrum of each VPO compound, it will be useful to consider the NMR spectrum of V_2O_5. Like the two model compounds which are thought to be representative of the actual catalysts, V_2O_5 contains VO_6 pseudooctahedra. An idealized structure is shown in Figure 7a. The vanadyl bond (V=O) has a length of 1.54 A and is roughly perpendicular to the plane of the figure, while the four equatorial V-O bond lengths are 1.78, 1.88, 1.88 and 2.02 A (43). Adjacent layers are joined through V=O-V bonding, in which the long V-O bond is 2.81 A. The structure in Figure 7b, in which the long V-O bonds are omitted, shows how the layers are joined.

From the apparent equivalence of the vanadium atoms and the distortion of the VO_6 groups from octahedral symmetry, one would expect the NMR spectrum to be that of a single type of vanadium showing at least first order effects of the quadrupolar interaction. This is in fact what has been observed, although the quadrupolar coupling (e^2qQ/h) is only 800 kHz

Table 2. ^{51}V NMR Results for VPO Catalysts

	intensity[a], shift[b] and width[c]
β-$VOPO_4$	
untreated	s[$\sigma_\perp$ -175, $\sigma_\parallel$ +2200] m[-150 (3)] m[-1050 (5)]
butane-treated	s[$\sigma_\perp$ -210, $\sigma_\parallel$ -930] m[+155 (4)] m[$\sigma_\perp$ +1015, $\sigma_\parallel$ +600]
butene-treated	no signal
$(VO)_2P_2O_7$	
untreated	no signal
butane-treated	no signal
butene-treated	no signal
precatalysts	
P/V = 0.9	w[$\sigma_\perp$ -315, $\sigma_\parallel$ -1000]
P/V = 1.0	no signal
P/V = 1.1	no signal
B phase catalysts	
P/V = 0.9	
untreated	s[$\sigma_\perp$ -295, $\sigma_\parallel$ -440] ww[+1150 (20)]
butane-treated	m[$\sigma_\perp$ -250, $\sigma_\parallel$ -330] m[+260 (20)]
P/V = 1.0	
untreated	m[-210 (7)]
butane-treated	w[$\sigma_\perp$ -440, $\sigma_\parallel$ -1200]
P/V = 1.1	
untreated	no signal
butane-treated	ww[-750 (60)]

[a] S, m, w and ww denote intensities from strong to very weak.
[b] Shifts are in ppm relative to $NH_4VO_{3(aq)}$ using the σ convention.
[c] For symmetric peaks, the FWHM in kHz is in parentheses.

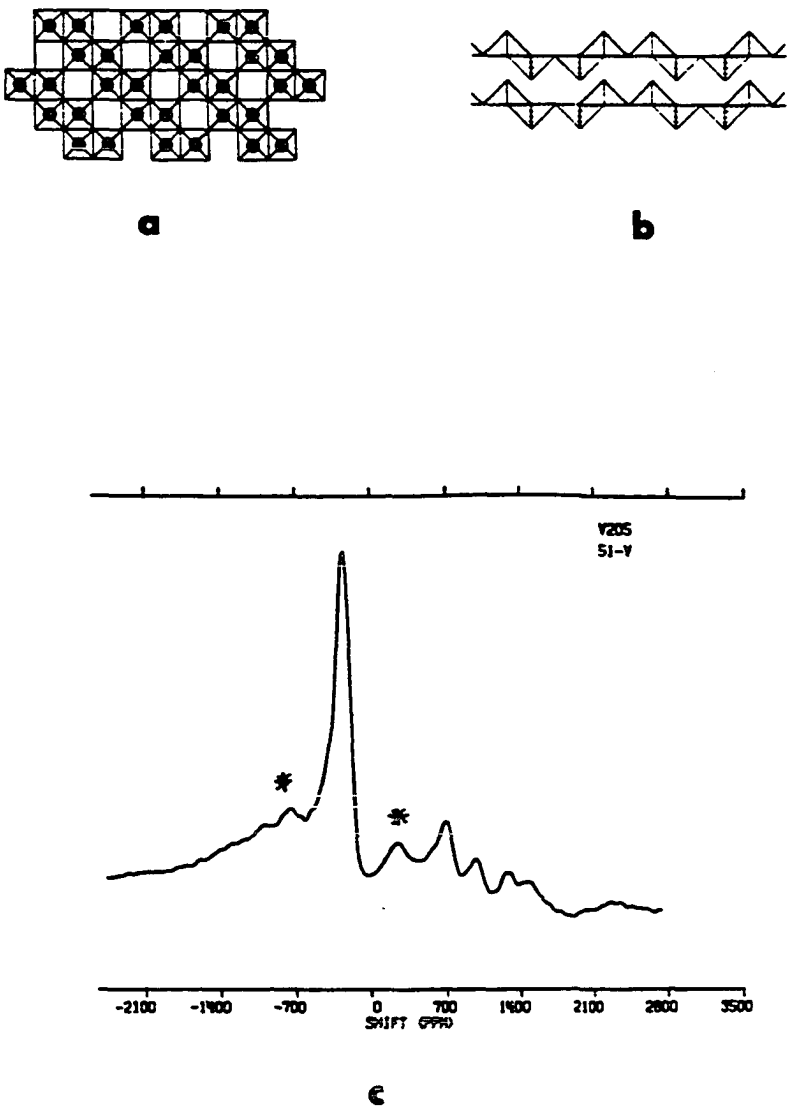

Figure 7. Idealized structures of V_2O_5, a) viewed perpendicular to a layer, b) viewed end-on to a layer (the long V-O bonds have been omitted)(43), and c) the 51-V NMR spectrum of V_2O_5.

and the line shape of the central transition is dominated by chemical shift anisotropy rather than second order quadrupolar effects (40,41,44,45). From a single crystal study, the principal values of the chemical shift tensor were found to be 180, -650 and 300 ppm relative to aqueous Na_3VO_4 (41), while a powder study showed axial symmetry and values of $\sigma_{\parallel}$ = -350 ppm and $\sigma_{\perp}$ = 200 ppm relative to aqueous $NaVO_3$ (40).

The spectrum of V_2O_5 obtained in this laboratory is shown in Figure 7c. The two peaks marked with a star are centered about the intense peak at -225 ppm, and their separation of 57 kHz corresponds to the reported e^2qQ/h of 800 kHz. Aside from these three peaks, which are the central and innermost satellite transitions of a first order quadrupolar powder pattern, the other spectral features are unexpected. Perhaps one or more pairs of the unexpected features are part of a central transition powder pattern. An NMR spectrum was recorded at a lower magnetic field (in which ^{51}V resonated at 14 MHz) to determine if any of the features shifted in a way characteristic of the second order quadrupolar interaction, but comparison with the high field spectrum was inconclusive. The results from x-ray powder diffraction indicate that something other than V_2O_5 is in the sample, but the impurity was not identifiable as any other known vanadium - oxygen phase (46). Similar NMR results were obtained regardless of whether the V_2O_5 examined came from Fisher Scientific (100.4%) or was prepared by heating NH_4VO_3 in oxygen at 500°C. (47).

Allersma et al. (48) determined through magnetic susceptibility measurements that a V_2O_5 powder from Fisher was actually $V_2O_{4.9}$, and that the crystalline V_2O_5 contained V(IV) as defects, with the concentration depending on method of preparation. Indeed, the results of EPR spin counting (vide infra) on the V_2O_5 used here indicated about 7×10^{18} V(IV) per gram. Since the four NMR peaks upfield of 600 ppm are out of the range of shifts expected for vanadium coordinated by oxygen, it is reasonable to interpret these features as dipolar shifted resonances that result from vanadium at or near crystalline defects.

The ^{51}V NMR spectrum of the model compound vanadyl phosphate, β-$VOPO_4$, is shown in Figure 8a. Two moderately intense narrow peaks appear at -150 ppm and -1050 ppm, with full width at half maximum (FWHM) of 3 kHz and 5 kHz, respectively. These two narrow peaks are superimposed on what conceivably could be an axially symmetric chemical shift tensor, with $\sigma_\perp$ being the intense peak at -175 ppm, and $\sigma_\parallel$ being about +2200 ppm. Alternatively, the very broad signal could be a symmetric peak centered at about +1000 ppm. Another broad peak appears at -1250 ppm, with FWHM 25 kHz.

Two idealized structures of β-$VOPO_4$ are shown in Figure 9. V(V) occurs in chains of corner-sharing VO_6 pseudooctahedra which are joined by PO_4 tetrahedra that share oxygen atoms with four separate VO_6 units in three different chains. Gopal and Calvo (34) report the equatorial bond lengths in the VO_6 units as 1.85, 1.89, 1.89 and 1.90 A, the V=O bond

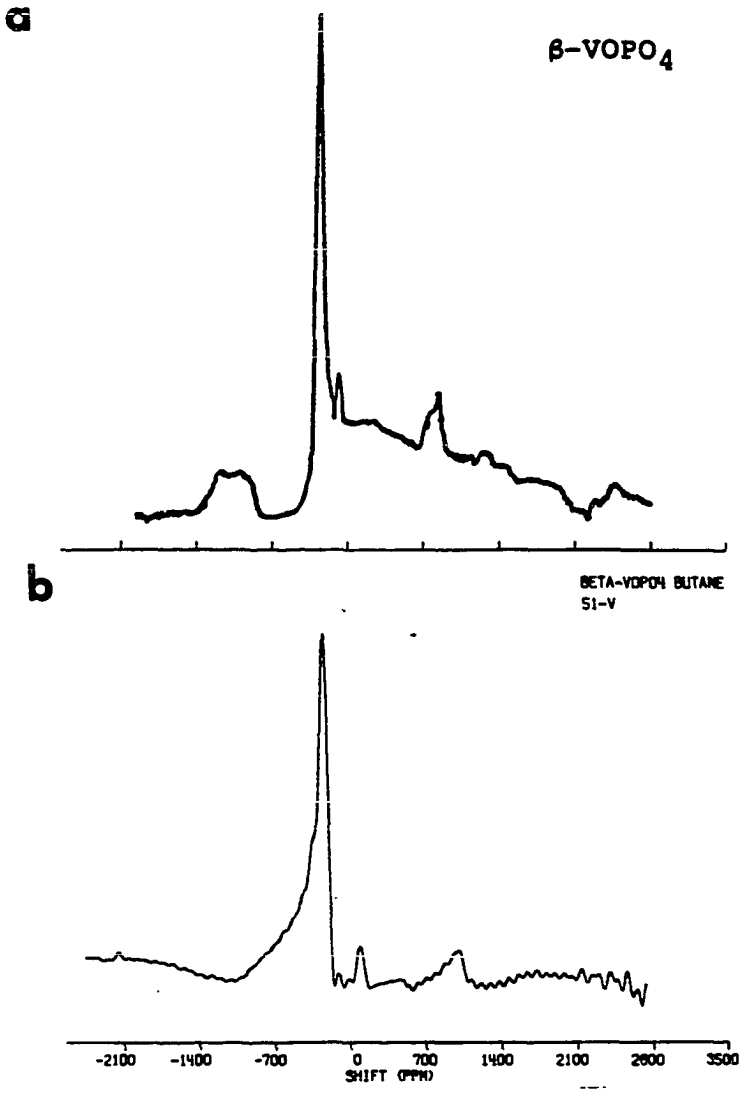

Figure 8. ^{51}V NMR spectra of β-$VOPO_4$ a) untreated, and b) treated with butane.

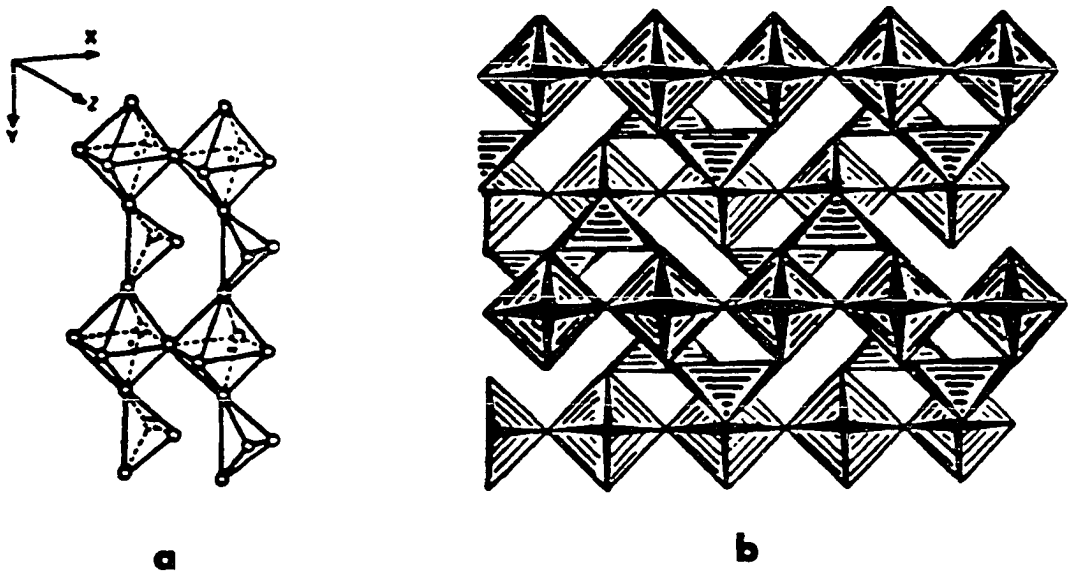

Figure 9. Idealized structures of β-$VOPO_4$, showing a) a three-dimensional representation (10), and b) a projection onto the xz-plane (49).

length as 1.56 A and the long V-O bond length as 2.59 A. The VO_6 units in this compound seem to be less distorted than those in V_2O_5, and it is perhaps surprising that the spectrum does not show a first order quadrupolar powder pattern with a small splitting. The most intense peak is due to vanadium in the known VO_6 units, while the peak at -175 ppm must be due to some unpredicted type of vanadium. The features at -1250 ppm and +2200 ppm are probably dipolar shifted peaks associated with crystalline defects.

Figure 8b shows the spectrum of β-$VOPO_4$ after exposure for 18 hours at 450°C. to a stream of 1.5% butane in air. The three most prominent peaks in the spectrum of the untreated model compound remain, while the two broad features have disappeared. The intense peak at -210 ppm now appears to be part of an axially symmetric tensor with $\sigma_{\parallel}$ at -930 ppm, downfield instead of upfield as proposed for the untreated compound. The small peak at +155 ppm is symmetric with FWHM 4 kHz, and the small peak further upfield seems to be a shift tensor with $\sigma_{\perp}$ = +1015 ppm and $\sigma_{\parallel}$ = +600 ppm.

The spectrum of β-$VOPO_4$ after exposure to 1-butene (1.5% in air for 18 hours at 450°C.) showed no signal that could be attributed to the sample. The quadrupole interaction is unlikely to be the cause of the disappearance of the signal; both the untreated and butane treated compounds yielded distinct NMR signals, and it is not reasonable to expect that exposure to butene could induce structural distortions in the bulk large enough to have such a drastic effect on the spectrum. On the other hand, the butene exposure should reduce at least some of the V(V) to paramagnetic V(IV) (35), and the signal has probably been broadened beyond visibility through interaction with unpaired electron spin. Perhaps the only question that remains is whether all vanadium has been reduced, or if some vanadium has remained as V(V) but is undetectable due to the proximity of V(IV).

The model compound vanadyl pyrophosphate, $(VO)_2P_2O_7$, did not give a ^{51}V NMR signal, either untreated or treated with

butane or butene as described above. The absence of a signal can be explained by the same considerations discussed for β-$VOPO_4$ exposed to butene. In this compound, vanadium is nominally all V(IV) even before hydrocarbon treatment, and the possibility of extreme broadening due to unpaired electron spin is very likely.

The only precatalyst to give a ^{51}V signal was the one with P/V = 0.9 (Figure 10a). The weak signal has roughly the appearance of an axially symmetric chemical shift tensor with $\sigma_\perp$ = -315 ppm and $\sigma_\parallel$ = -1000 ppm, which is consistent with reported results for V(V) in VO_6 pseudooctahedra (39). Since the precatalysts are in a highly reduced state (38), broadening due to unpaired electron spin is likely.

The ^{51}V spectra of the B phase catalysts with P/V = 0.9 and 1.0 are shown in Figures 10b,c. For B phase 0.9, an intense axially symmetric shift tensor from V(V) in the common VO_6 unit is observed but with a smaller anisotropy than in the case of the precatalyst 0.9. There is also a hint of a broad peak at +1150 ppm, which could come from V(IV) or perhaps a V(V) very near a V(IV). The spectrum of B phase 1.0 is much less intense than the spectrum of B phase 0.9. The most obvious peak is located at -210 ppm and is symmetric with FWHM 7 kHz. Another peak appears at +1180 ppm, with FWHM 4 kHz. As in the spectrum of β-$VOPO_4$, there seems to be a very broad signal in between these two narrow peaks. No signal was observed from B phase 1.1. The B phase catalysts are amorphous to a significant degree, and

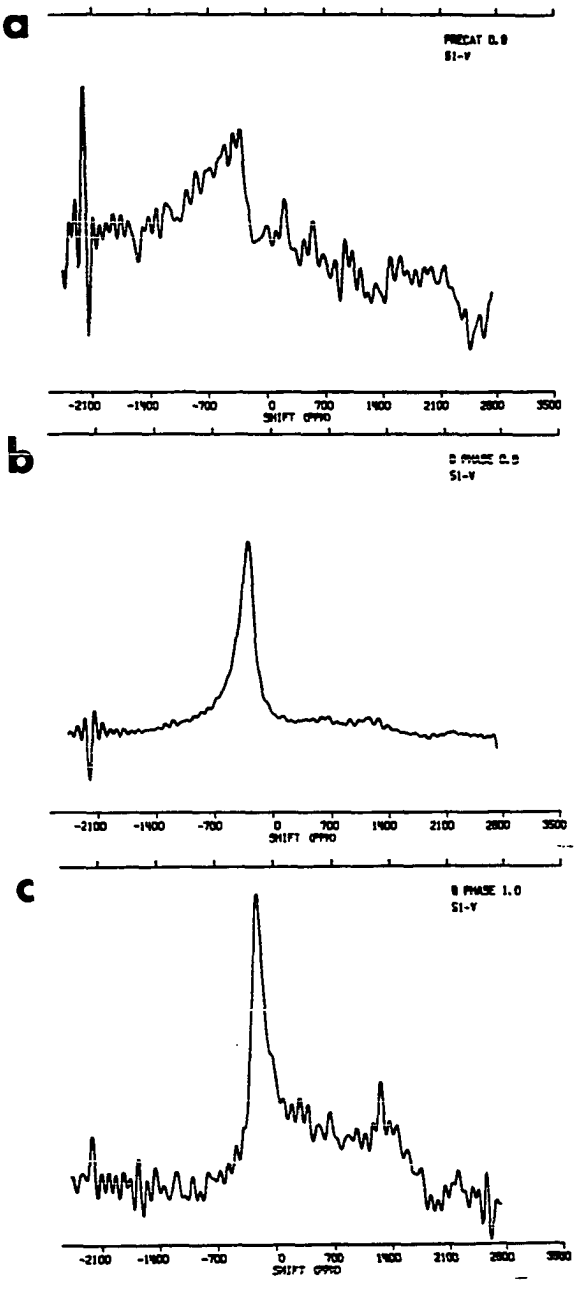

Figure 10. ^{51}V NMR spectra of a) precatalyst P/V = 0.9 b) B phase P/V = 0.9, untreated, and c) B phase P/V = 1.0, untreated.

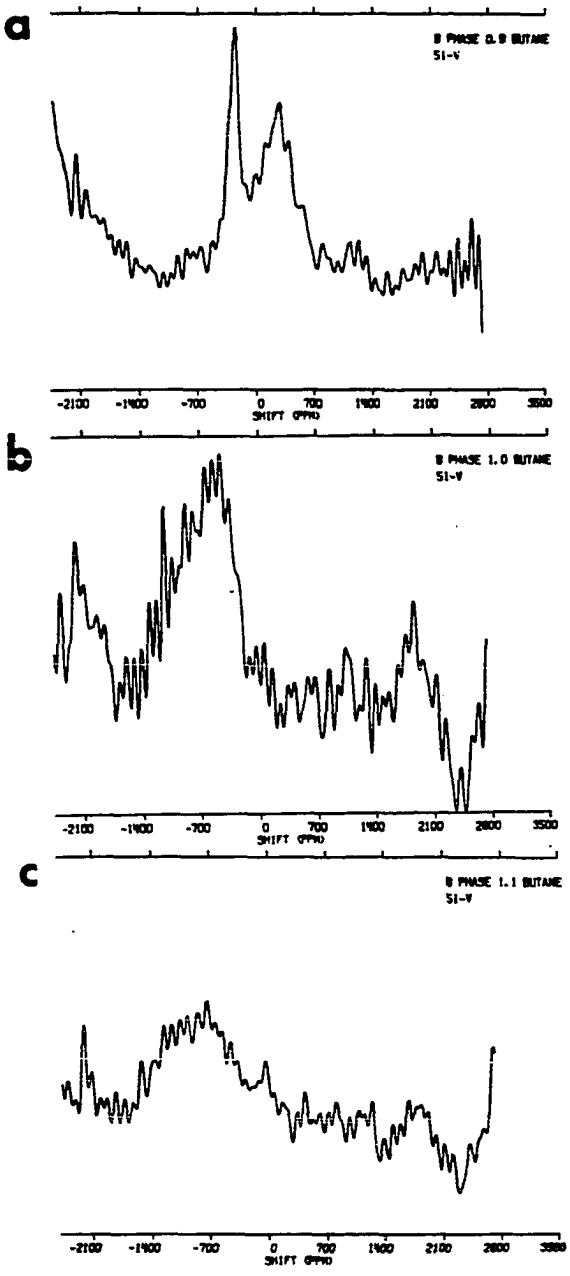

Figure 11. ^{51}V NMR spectra of B phase catalysts after treatment with butane a) P/V = 0.9 b) P/V = 1.0 c) P/V = 1.1.

severe quadrupolar broadening must be considered as a cause for detecting no signal as well as the effects of unpaired electron spin.

After exposure to a stream of 1.5% butane in air at 450°C. for 18 hours, the B phase compounds give different ^{51}V spectra. The spectrum of B phase 0.9 (Figure 11a) has become less intense. The most prominent feature is still an axially symmetric shift tensor, with $\sigma_{\perp}$ = -250 ppm and $\sigma_{\parallel}$ = -330 ppm, that is attributed to V(V) in the common VO_6 units. This tensor has an even smaller anisotropy than the one displayed by the untreated B phase 0.9. A somewhat weaker peak also occurs at +260 ppm. The only feature visible in the spectrum of B phase 1.0 after butane exposure (Figure 11b) is a very weak axially symmetric tensor with $\sigma_{\perp}$ = -440 ppm and $\sigma_{\parallel}$ = -1200 ppm. For the B phase 1.1 catalyst, a very weak signal is now apparent (Figure 11c). Unlike the weak signal from B phase 1.0, this peak is roughly symmetric and is centered at about -750 ppm with a FWHM of perhaps 60 kHz. This could be due to a small concentration of V(V) in VO_6 that is broadened almost to the point of invisibility.

ELECTRON PARAMAGNETIC RESONANCE

General Considerations

Electron paramagnetic resonance spectroscopy is based on the absorption of microwave radiation by materials having electrons with unpaired spins. The most fundamental equation of the EPR phenomenon is the one describing the Zeeman interaction between the electron spin magnetic moment and a magnetic field: $\hat{H} = g\beta H_z \hat{S}_z$, where β is the Bohr magneton for the electron, H_z the applied magnetic field and $\hat{S}_z$ the component of electron spin angular momentum in the direction of the magnetic field. Differences in the frequency of the transition between the two possible electron spin states are customarily described by changing the g factor in the equation. The deviation of the g factor from the free electron value of 2.002 is caused by the coupling of orbital angular =momentum with spin angular momentum, and is anisotropic when the paramagnetic atom is in a site with symmetry lower than spherical or cubic.

The EPR linewidths in solids are primarily influenced by two interactions (50-52). The dipolar coupling between the magnetic moments of neighboring electrons leads to linewidths comparable to β/r^3, where r is the nearest-neighbor distance. Coulombic interactions between the electrons of neighboring atoms lead to exchange coupling, which has the form $H_{eij} = -2J_{ij}\vec{S}_i \cdot \vec{S}_j$, where J_{ij} is the exchange integral. Because of the dependence on J, if the wave functions for the

two electrons do not overlap, there will be no exchange interaction. In the case where the EPR signal is split due to the hyperfine interaction with the nucleus, the exchange coupling can cause broadening. Depending on the relative strengths of the hyperfine and exchange interactions, the individual lines may appear broadened or may coalesce into a single broad line. For the extreme of a very strong exchange interaction, an EPR line will be narrowed. In terms of the Van Vleck moment analysis, the exchange interaction increases the fourth moment of the line while leaving the second moment unaffected. The resulting lineshape has a narrowed central portion and extremely wide wings, which are effectively invisible.

The EPR of V(IV) is well-known in the literature of catalysis (53-60). In the absence of anisotropy, the g value ranges from 1.960 to 1.970 (53-57) and linewidths range from 75 to 250 gauss (54-57). When anisotropy is present, $g_{\perp}$ falls in the range 1.979 to 1.982 and $g_{\parallel}$ in the range 1.928 to 1.938 (55-57); these g values are typical for vanadyl complexes with axial symmetry (58). In vanadium-phosphorous catalysts the signal was observable at room temperature. Hyperfine structure was seen in only a few cases - for a VPO catalyst with P/V=1.0 (57), for VPO catalysts with P/V=0.5, 0.8 (54) and for α-$VOPO_4$ $2H_2O$ (55). The general absence of hyperfine structure is attributed to the dipolar interaction (55) or the exchange interaction (53-55,58). Linewidths greater than 250 Gauss are attributed to a distribution of

ill-defined symmetries throughout the sample (57) or exchange coupling of V(IV) with high spin V(III) (58).

Pepera et al. (5) looked for a half-field signal from a $\Delta m_s = \pm 2$ transition that would indicate the presence of a triplet state resulting from antiferromagnetic coupling of spins associated with adjacent V(IV) vanadyl groups. They were successful in detecting this signal at room temperature in a freshly calcined sample of β-$(VO)_2P_2O_7$; the intensity of this signal was about $1/500^{th}$ the intensity of the $\Delta m_s = \pm 1$ transition.

In all known cases, the zero field splitting of V(III) is large, and the $\Delta m_s = \pm 1$ transition has only been observed by using an unusually strong magnetic field (27). In a few cases, the $\Delta m_s = \pm 2$ forbidden transition has been observed. Previous studies of catalysts commonly employed chemical analysis for the detection of V(III) (59,60).

Experimental Procedure

Electron paramagnetic resonance experiments were performed on a Bruker ER-220-D-SR spectrometer equipped with a Nicolet 535 signal averager. All experiments were performed at room temperature. Spin counting was performed by instrumental double integration of the derivative spectra using copper sulfate pentahydrate as a standard. Spectra were recorded under varying conditions, and the following equation was employed to take into account the effect of these differences on the measured peak areas (52):

$$\text{area}_x = \frac{\text{gain}_x}{\text{gain}_s} \frac{\text{mod.amp.}_x}{\text{mod.amp.}_s} \left(\frac{\text{power}_x}{\text{power}_s}\right)^{1/2} \left(\frac{\text{sweep width}_s}{\text{sweep width}_x}\right)^2 \frac{g_x}{g_s} \quad (\text{area}_s)$$

where x refers to the unknown and s to the standard.

Results

Each of the three precatalysts P/V = 0.9, 1.0 and 1.1 gave an isotropic peak about 70 Gauss wide at g = 1.970. With the exception of the B phase 1.0 catalyst before treatment with butane, all of the B phase catalysts, both before and after exposure to butane, gave isotropic peaks with a g value of about 1.970. Widths were about 100 Gauss, except for B phase 1.1 after butane treatment, where the width was 150 Gauss. All of the other catalysts gave axially symmetric EPR signals, with $g_\perp$ and $g_\parallel$ consistent with the range for V(IV) reported in the literature (53-57).

The absence of hyperfine splitting in the EPR spectra of these catalysts is attributed to either the exchange interaction or the dipolar interaction or both. In either case, the paramagnetic sites must be quite close, and the absence of resolved hyperfine structure may be an indication of the existence of clusters of V(IV).

The results of EPR spin counting are shown in Table 3. The EPR signals obtained represent only V(IV) and the spin counts are thus a direct measure of the concentration of V(IV). The amount of V(IV) as a fraction of total vanadium is also shown. For the model catalysts, the total number of

Table 3. Summary of EPR Spin Counting Results

	V(IV), atoms/gram	V(IV), % of total V
V_2O_5	7×10^{18}	0.09
$(VO)_2P_2O_7$		
untreated	3.1×10^{21}	79
butane-treated	1.0×10^{21}	26
butene-treated	0.91×10^{21}	23
β-$VOPO_4$		
untreated	0.25×10^{21}	7
butane-treated	0.33×10^{21}	9
butene-treated	1.5×10^{21}	41
precatalysts		
P/V = 0.9	3.0×10^{21}	71
P/V = 1.0	3.5×10^{21}	92
P/V = 1.1	2.1×10^{21}	62
B phase catalysts		
P/V = 0.9		
untreated	0.66×10^{21}	24
butane-treated	0.81×10^{21}	29
P/V = 1.0		
untreated	1.3×10^{21}	52
butane-treated	0.18×10^{21}	7
P/V = 1.1		
untreated	1.4×10^{21}	41
butane-treated	0.13×10^{21}	4

vanadium atoms per gram was estimated from the chemical formula (3.9 and 3.7 x 10^{21} V atoms/g, for vanadyl pyrophosphate and vanadyl phosphate, respectively). In the case of the precatalysts, the compound with P/V = 1.0 was assumed to have 3.8 x 10^{21} V atoms/g; this figure was raised by 10% for the compound with P/V = 0.9 and lowered by 10% for P/V = 1.1. The figure for the B phase 1.0 catalyst was obtained by correcting 3.8 x 10^{21} for the reported ~33% loss of phosphorous during activation in air (38). For the other two B phase catalysts, the difference in P/V was accounted for as described for the precatalysts after taking into account the phosphorous losses of 33% and 0% for P/V = 0.9 and 1.1, respectively.

The amounts of V(IV) as a fraction of total vanadium can be divided into three ranges: high (>60%), low (<10%) and middle (between 10% and 60%). Since $(VO)_2P_2O_7$ is nominally all V(IV), the spin counting was expected to show that 100% of the vanadium was V(IV). The absolute number of spins is considered to be uncertain by about 25%, so the discrepancy between 100% and the measured value of 79% may not be real. On the other hand, Pepera et al. (5) reported that 20% of the vanadium in a freshly calcined sample of β-$(VO)_2P_2O_7$ is V(V).

In vanadyl phosphate, the vanadium is nominally V(V), and the spin concentration in β-$VOPO_4$ is correspondingly low. The exposure to butane increases the V(IV) concentration only slightly, by an amount that is within the uncertainty in the repeatability of the measurement ($\pm$5%). Exposure to butene,

which is considered to be more reducing than butane, results in a six-fold increase in concentration of unpaired spins. For vanadyl pyrophosphate, both butane and butene treatments reduce the fraction of V(IV) by a factor of 4. If the effect of the hydrocarbon treatment is reduction of the catalyst, then the decrease in V(IV) is reasonable; the signal intensity has decreased because the V(III) formed gives no EPR signal.

The precatalysts are reported to be in a highly reduced state (38), and this is reflected by the high fractions of V(IV) found. Since the higher P/V ratios are known to stabilize V(IV) over V(V), it is perhaps surprising that the precatalyst with P/V = 1.1 has a lower fraction of V(IV) than the other two precatalysts. If the precatalysts with higher P/V stabilize any reduced form, rather than simply V(IV), then the relatively low V(IV) fraction of precatalyst 1.1 may plausibly be an indication of the presence of V(III). From the EPR results alone, it is impossible to determine whether the fraction of vanadium that is not V(IV) is V(III) or V(V).

There is also a decrease in fraction of V(IV) as P/V increases from 1.0 to 1.1 in the B phase catalysts, and the probable cause is the same as that described for the precatalysts. The B phase 0.9 catalyst has a relatively low fraction of V(IV), but in this case the remainder of the vanadium is more likely to be V(V). As in the case of β-$VOPO_4$, the butane treatment increased the fraction of V(IV) by an almost insignificant amount in B phase 0.9. B phases 1.0 and

1.1 have a relatively high concentration of V(IV) before exposure to butane, and a considerably lower concentration after exposure to butane. Again, this is more likely to be due to the reduction of V(IV) to V(III), rather than to an increase in fraction of V(V).

DISCUSSION

The most important influence on the ^{31}P and ^{51}V NMR spectra of the VPO catalysts is the effect of unpaired electron spins. Shifts in the frequency of absorption and line broadening, both moderate and severe, are a result of the interaction of the nuclei with unpaired electron spins. Since NMR signals are detected in most samples, it will be assumed that the condition $1/T_{1e} >> A_H$ holds for all interacting pairs of electrons and nuclei in all samples. Furthermore, it will be assumed that all unpaired electron spin is localized in the 3d orbitals of vanadium atoms. The strength of the interaction, then, is taken to depend only on the distance between the electron spin and the nucleus.

At one extreme, the electron - nucleus separation is so small that the NMR absorption is broadened beyond observability by strong dipolar coupling. This is the case for the ^{51}V spectrum of $(VO)_2P_2O_7$ and the ^{31}P spectra of B phases 1.0 and 1.1 after treatment with butane. At the other extreme, the concentration of unpaired spins is so low that there is no detectable effect on the spectrum. In this category is the ^{31}P spectrum of β-$VOPO_4$, in which no paramagnetically shifted peak is observed and the linewidth of the lone peak is attributable to homonuclear and heteronuclear dipolar broadening. Between these two extremes are most of the spectra, in which there are dipolar shifted peaks and broadening due to electron - nucleus dipolar interactions.

Table 4 summarizes the results of EPR spin counting, ^{31}P NMR and ^{51}V NMR experiments. The NMR spectra have been considered in the context of the strength of the electron - nucleus interaction suggested by linewidths, intensities and shifts of peaks. The EPR spin counting results have been classified as strong, weak or moderate as defined in the discussion of the EPR data in the preceding section.

In spite of the fact that the vanadium in the model catalyst β-$VOPO_4$ is nominally all V(V), the EPR results indicate that a small concentration of V(IV) is present. The V(IV) concentration is low enough, or perhaps localized enough, that it has no apparent effect on the ^{31}P spectrum. The effect of V(IV) on the ^{51}V spectrum is greater; the peak representing unaffected vanadium is very intense, but there are also two weaker peaks from affected vanadium.

In the model compound $(VO)_2P_2O_7$, the vanadium is nominally all V(IV). The EPR results indicate a high concentration of V(IV), and the absence of a ^{51}V NMR signal supports this. In principle, NMR signals from V(IV) can be observed. Landsberger and Bray (61) reported a 200 kHz wide V(IV) peak at 16 MHz in a V_2O_5-P_2O_5 glass. Since the anisotropic hyperfine (pseudocontact) interaction is proportional to field strength, the same linewidth at 57 MHz (where the present work was conducted) would be 800 kHz (~14,000 ppm), which is too broad to be observed. Also consistent with the presence of V(IV) are the dipolar shifted peaks and low intensity of the ^{31}P NMR spectrum. The unshifted phosphorous peak may be

Table 4. The Effects of Unpaired Electron Spin on the Magnetic Resonance of VPO Catalysts

	Strength of effects of unpaired electrons		
	^{31}P NMR	^{51}V NMR	EPR spin count
β-$VOPO_4$			
untreated	none	moderate	weak
butane-treated	v. weak	moderate	weak
butene-treated	weak	v. strong	moderate
$(VO)_2P_2O_7$			
untreated	strong	v. strong	strong
butane-treated	strong	v. strong	moderate
butene-treated	strong	v. strong	moderate
precatalysts			
P/V = 0.9	moderate	strong	strong
P/V = 1.0	moderate	v. strong	strong
P/V = 1.1	moderate	v. strong	strong
B phase catalysts			
P/V = 0.9			
untreated	v. weak	v. weak	moderate
butane-treated	v. weak	weak	moderate
P/V = 1.0			
untreated	moderate	moderate	moderate
butane-treated	v. strong	strong	weak
P/V = 1.1			
untreated	moderate	v. strong	moderate
butane-treated	v. strong	v. strong	weak

an indication of the existence of a polycondensed phosphate domain, or perhaps a domain containing only V(V).

Exposure to a stream of 1.5% n-butane in air at 450°C. for 18 hours has only a small effect on β-$VOPO_4$. The ^{31}P and ^{51}V NMR spectra are almost unchanged, while the EPR results show a slight increase in the concentration of V(IV). Butane exposure had a more significant effect on $(VO)_2P_2O_7$. The continued absence of a ^{51}V signal and disappearance of the shifted peaks in the ^{31}P spectrum imply even stronger effects of unpaired spins, but the EPR spin counting shows a decrease in concentration of V(IV). These results suggest that a large fraction of the V(IV) in $(VO)_2P_2O_7$ has been reduced to V(III) by exposure to butane.

A similar treatment with 1-butene has the same effect on $(VO)_2P_2O_7$ as the butane treatment. However, for β-$VOPO_4$, butene had a larger effect than butane. EPR spin counting showed a large increase in V(IV) that was also suggested by the disappearance of ^{51}V NMR signals and a decrease in intensity and broadening of the ^{31}P peak.

The ^{51}V spectra of the precatalysts demonstrate the increasingly important effects of unpaired electron spin at higher values of P/V. The ^{51}V spectrum of precatalyst 0.9 shows a very weak unshifted signal, indicating only a small amount of relatively unaffected vanadium, while the ^{51}V spectra of precatalysts 1.0 and 1.1 show no signal, indicating the lack of any unaffected vanadium.

The ^{31}P spectra, on the other hand, have a dipolar shifted peak that decreases in intensity as P/V increases. Given the stabilization of V(IV) at higher values of P/V, one might have expected that as P/V increased, the dipolar shifted ^{31}P peak would increase in area as the increasing concentration of V(IV) affected more ^{31}P nuclei. In this case, a different process would seem to be dominant as P/V increases. X-ray diffraction experiments indicate that the crystal structures of each of the precatalysts are identical but somewhat amorphous at P/V = 1.1 (38), which suggests that the excess phosphorous at high P/V might dilute the effects of unpaired spin, possibly by increasing interlayer distances. Perhaps the relative decrease in area that has been observed indicates that the increasing V(IV) concentration affects more strongly the ^{31}P already affected to the extent that some of the signal becomes broadened beyond visibility. The unshifted peak, which remains unaffected by the increasing V(IV) concentration, may be a result of an isolated domain of either polycondensed phosphates or a VPO structure with only V(V).

The EPR spin counting results indicate that the V(IV) concentration of precatalyst 1.1 is small relative to that of precatalysts 0.9 and 1.0. Given the trend in areas in the ^{31}P spectra, it is important to recognize that in this case the low V(IV) concentration might be an indication that much of the vanadium occurs as V(V) in precatalyst 1.1. However, the lack of ^{51}V signal from this compound does not provide

convincing support for this conjecture. Keeping in mind the known stabilization of reduced states of vanadium at high P/V, it seems more likely that the low V(IV) concentration occurs because of the existence of V(III). This would not be inconsistent with the proposed explanations for the trend in ^{31}P areas.

In agreement with the known increase in stabilization of V(IV) at high phosphorous to vanadium ratios, the B phase catalysts give spectra that are increasingly affected by unpaired spins as P/V increases. The relative intensity of the dipolar shifted ^{31}P resonance goes from 0% to 12% to 75% as P/V increases from 0.9 to 1.0 to 1.1, while the intensity of the ^{51}V signals drop from strong to weak to zero. The trend is continued by the EPR spin counting results, which show an increase in V(IV) concentration as P/V increases.

Exposure to a stream of 1.5% n-butane in air at 450°C. for 18 hours increases the effects of unpaired spin in most cases. The single unshifted peak in the ^{31}P spectrum of B phase 0.9 remains after butane exposure, but all of the ^{31}P signal from B phases 1.0 and 1.1 is destroyed. The ^{51}V signal is decreased in the spectra of B phases 0.9 and 1.0, but increased in the spectrum of B phase 1.1. This unexpected increase is only from an undetectable signal to an extremely weak signal and may not even be real. With the exception of this anomalous weak signal, the spectra of the B phase compounds after butane treatment still reflect the increase in stabilization of reduced vanadium at higher P/V.

Aside from contributing to knowledge of vanadium oxidation states, the results of magnetic resonance experiments provide some clues about how the structures of the different VPO compounds change with use in the conversion of n-butane or 1-butene to maleic anhydride. Earlier studies using x-ray diffraction, Fourier transform infrared, laser Raman and photoelectron spectroscopies indicated that treatment with n-butane left β-$VOPO_4$ unchanged except for the formation of some V(IV) on the surface (35). The NMR results also suggest that the structure is unchanged. The slight increase in V(IV) detected by the EPR spin counting is about an order of magnitude larger than the number of vanadium atoms expected to be found at the surface for β-$VOPO_4$ with the surface area of this sample (~2 m^2/g).

Exposure to 1-butene converted β-$VOPO_4$ to $(VO)_2P_2O_7$, with both V(V) and V(IV) on the surface (35). EPR spin counting results clearly indicate that large-scale conversion of V(V) to V(IV) has occurred. However, the ^{31}P NMR spectrum of β-$VOPO_4$ after butene treatment is not identical to that of $(VO)_2P_2O_7$. None of the downfield peaks in the spectrum of $(VO)_2P_2O_7$ are present in the spectrum of β-$VOPO_4$ after butene treatment.

In the case of $(VO)_2P_2O_7$, previous studies have shown that exposure to n-butane and 1-butene leaves the structure unchanged but forms some V(V) on the surface (35). Just as in the case of β-$VOPO_4$ after butene exposure, all the peaks but the one at ~0 ppm are absent. Thus it would appear that

some change has occurred in the catalyst with use.

Each of the three precatalysts studied has the same x-ray diffraction pattern (38). However, the NMR spectra are somewhat different. In the ^{31}P spectra, the same two peaks occur for each P/V ratio, but the relative areas are different. The differences in the ^{51}V spectra are perhaps almost insignificant; the precatalyst 0.9 gives a very weak and broad signal. Based on the more detailed discussion of the precatalysts given above, it would seem that a significant change in concentration of unpaired spins occurs as P/V changes, but without any major structural modifications.

After calcination in air for three hours at 380°C., the precatalysts become B phase compounds. The B phases with P/V = 1.0 and 1.1 have the same structure as the precatalysts as determined by x-ray diffraction (38), but again the two peaks in the ^{31}P spectra, which correspond to those observed in the precatalysts, have different relative areas for the different values of P/V. The ^{51}V spectra are somewhat different, also. The B phase 1.0 gives a weak spectrum with at least two features, while the B phase 1.1 gives no signal. The B phase 0.9 has a different structure, known as B' (38), and the NMR spectrum is different than those for B phases 1.0 and 1.1. Of all the compounds studied, the one having the NMR spectrum most similar to B phase 0.9 is β-$VOPO_4$.

According to previous studies, the structures of the B phase catalysts change after exposure to 1.5% n-butane in air for 18 hours at 450°C.: B phase 0.9 becomes α-$VOPO_4$, and B

phases 1.0 and 1.1 become mixtures of α-$VOPO_4$ and $(VO)_2P_2O_7$ (38). The ^{51}V spectra of B phases 1.0 and 1.1 after exposure to butane are very similar, but do not seem to contain an observable contribution from the spectrum of B phase 0.9 after butane exposure (assumed to be the spectrum of α-$VOPO_4$). Similarly, the ^{31}P spectra of the exposed B phases 1.0 and 1.1 are the same (no signal was observed), but do not show any evidence of the spectrum from butane treated B phase 0.9.

The results of magnetic resonance experiments on VPO catalysts generally support the results obtained with other spectroscopic methods. In particular, the combination of ^{31}P, ^{51}V NMR and EPR spin counting provides the ability to infer the presence of V(III). Through the effects of unpaired electron spins on the NMR spectra, differences can be detected between some compounds that have been found to be identical using other methods. However, the amount of structural information obtainable from NMR is somewhat limited in the VPO system; the effects of unpaired electron spin mask potentially informative spectral features, such as the ^{31}P chemical shift anisotropies. The possibility exists that magnetic resonance may play an important role in elucidating correlations between structure and activity in VPO catalysts for the selective oxidation of butane and butene to maleic anhydride.

REFERENCES

1. Malow, M. Hydrocarbon Processing 1980, 149.
2. Moser, T. M.S. thesis, Iowa State University, Ames, Iowa, 1984.
3. Hodnett, B. Catal. Rev.- Sci. Eng. 1985, 27, 373.
4. Mars, P.; van Krevelen, D. Chem. Eng. Sci. 1954, 3(supplement), 41.
5. Pepera, M.; Callahan, J.; Desmond, M.; Milberger, E.; Blum, P.; Bremer, N. J. Am. Chem. Soc. 1985, 107, 4883.
6. Cavani, F.; Centi, G.; Manenti, I.; Trifiro, F. Ind. Eng. Chem. Prod. Res. Dev. 1985, 24, 221.
7. Hodnett, B.; Delmon, B. Appl. Catal. 1984, 9, 203.
8. Hodnett, B.; Delmon, B. J. Catal. 1984, 88, 43.
9. Poli, G.; Resta, I.; Ruggeri, O.; Trifiro, F. Appl. Catal. 1981, 1, 395.
10. Bordes, E.; Courtine, P. J. Catal. 1979, 57, 236.
11. Bordes, E.; Courtine, P. J. Chem. Soc., Chem. Commun. 1985, 294.
12. Johnson, J.; Johnston, D.; Jacobson, A.; Brody, J. J. Am. Chem. Soc. 1984, 106, 8123.
13. Bordes, E.; Courtine, P.; Johnson, J. J. Solid State Chem. 1984, 55, 270.
14. Cavani, F.; Centi, G.; Manenti, I.; Trifiro, F. Ind. Eng. Chem. Prod. Res. Dev. 1985, 24, 221.
15. Cavani, F.; Centi, G.; Trifiro, F. Appl. Catal. 1985, 15, 151.
16. Cavani, F.; Centi, G.; Trifiro, F. Appl. Catal. 1984, 9, 191.
17. Hodnett, B.; Delmon, B. J. Catal. 1984, 88, 43.
18. Hodnett, B.; Permanne, P.; Delmon, B. Appl. Catal. 1983, 6, 231.
19. Centi, G.; Trifiro, F. Appl. Catal. 1984, 12, 1.

20. Moser, T.; Schrader, G. J. Catal. 1985, 92, 216.

21. Wenig, R.; Schrader, G. To be published.

22. Drago, R. "Physical Methods in Chemistry"; W. B. Saunders: Philadelphia, 1977.

23. Swift, T. In "NMR of Paramagnetic Molecules"; La Mar, G.; Horrocks, W.; Holm, R., Eds.; Academic Press: New York, 1973; Chapter 2.

24. Jesson, J. In "NMR of Paramagnetic Molecules"; La Mar, G.; Horrocks, W.; Holm, R., Eds.; Academic Press: New York, 1973; Chapter 1.

25. Webb, G. Ann. Rep. on NMR Spectros. 1974, 6A, 1.

26. Kurland, R.; McGarvey, B. J. Magn. Reson. 1970, 2, 286.

27. Carlin, R. "Magnetochemistry"; Springer-Verlag: New York, 1986.

28. Mavel, G. Ann. Rep. on NMR Spectrosc. 1973, 5B, 1.

29. Duncan, T.; Douglass, D. Chem. Phys. 1984, 87, 339.

30. Grimmer, A. Spectrochim. Acta 1978, 34A, 941.

31. Duncan, T., personal communication.

32. Gerstein, B.; Chow, C.; Pembleton, R.; Wilson, R. J. Phys. Chem. 1977, 81, 565.

33. Wemmer, D. Ph.D. Thesis, University of California, Berkeley, California, 1973.

34. Gopal, R.; Calvo, C. J. Sol. St. Chem. 1972, 5, 432.

35. Moser, T., Department of Chemical Engineering, Iowa State University, Ames, Iowa, personal communication.

36. Middlemiss, N. Ph.D. Dissertation, McMaster University, Hamilton, Ontario, 1978.

37. Wustneck, N.; Wolf, H.; Seeboth, H. React. Kinet. Catal. Lett. 1982, 21, 497.

38. Wenig, R., Department of Chemical Engineering, Iowa State University, Ames, Iowa, personal communication.

39. Rehder, D. Bull. Magn. Reson. 1982, 4, 33.

40. Ragle, J. J. Chem. Phys. 1961, 35, 753.

41. Gornostansky, S.; Stager, C. J. Chem. Phys. 1967, 46, 4959.

42. Kidd, R. Ann. Rep. NMR Spectrosc. 1980, 10A, 1.

43. Wells, A. "Structural Inorganic Chemistry"; 5th ed.; Clarendon: London, 1962.

44. France, P. J. Magn. Reson. 1979, 34, 585.

45. France, P. J. Magn. Reson. 1980, 40, 311.

46. Benson, J., Ames Laboratory, Ames, Iowa, personal communication.

47. Prepared by T. Moser, Department of Chemical Engineering, Iowa State University, Ames, Iowa.

48. Allersma, T.; Hakim, R.; Kennedy, T.; Mackenzie, J. J. Chem. Phys. 1967, 46, 154.

49. Bordes, E.; Courtine, P.; Pannetier, G. Ann. Chim. 1973, 8, 105.

50. Abragam, A.; Bleaney, B. "Electron Paramagnetic Resonance of Transition Ions"; Clarendon: London, 1971.

51. Pake, G. "Electron Paramagnetic Resonance"; Elsevier: New York, 1969.

52. Wertz, J.; Bolton, J. "Electron Spin Resonance"; McGraw-Hill: New York, 1972.

53. Ballataud, D.; Bordes, E.; Courtine, P. "Solid State Chemistry 1982", proceedings of 2nd European Conference June, 1982.

54. Martini, G.; Morselli, L.; Riva, A.; Trifiro, F. React. Kinet. Catal. Lett. 1978, 8, 431.

55. Ballataud, D.; Bordes, E.; Courtine, P. Mater. Res. Bull. 1982, 17, 519.

56. Dyrek, K.; Serwicka, E.; Grzybowska, B. React. Kinet. Catal. Lett. 1979, 10, 93.

57. Martini, G.; Trifiro, F.; Vaccari, A. J. Phys. Chem. 1982, 86, 1573.

58. Nakamura, M.; Kawai, K.; Fujiwara, Y. J. Catal. 1974, 34, 345.

59. Dyrek, K.; Labanowska, M. J. Catal. 1985, 96, 32.

60. Bielanski, A.; Dyrek, K.; Serwicka, E. J. Catal. 1980, 66, 316.

61. Landsberger, F.; Bray, P. J. Chem. Phys. 1970, 53, 2757.

PART TWO. SELECTIVE AVERAGING OF THE SECOND ORDER QUADRUPOLAR INTERACTION IN ALUMINOSILICATES

INTRODUCTION

High resolution nuclear magnetic resonance of solids is generally difficult because of the line broadening effects of homonuclear and heteronuclear dipolar interactions and chemical shift anisotropy. Techniques have been developed to suppress the effects of these interactions: decoupling for the removal of dipolar interactions, rapid sample spinning at the magic angle for removal of chemical shift anisotropy and weak dipolar interactions, and multiple pulse sequences for the selective averaging of the homonuclear dipolar interaction. The development of these techniques led to considerable enhancement in the range of successful applications of NMR to the study of spin-1/2 nuclei in solids.

Nuclei with spin $I > 1/2$ are subject also to the quadrupole interaction. In the case of many systems of interest, such as aluminum-27 nuclei in zeolites, a distribution of large quadrupolar couplings causes all but one of the spectral features resulting from quadrupolar effects to be unobservable. The remaining feature is the absorption due to the central transition in the manifold of quadrupolar split energy levels of nuclear spin. In the context of a perturbation treatment, where the quadrupolar interaction is considered to be a perturbation on the Zeeman interaction, the central transition is shifted and broadened by second order effects. The line broadening can be large enough that

desirable information is lost through poor resolution of neighboring peaks.

Techniques exist for the suppression of line broadening due to the second order effects of the quadrupole interaction, but each has limited applicability. One method is to perform NMR experiments in an extremely high magnetic field (1-3). Since the strength of the second order quadrupole interaction is inversely proportional to the magnetic field, line broadening due to this interaction will be suppressed. Unfortunately, the chemical shift anisotropy is proportional to the magnetic field strength; consequently this kind of broadening may remain and be too large to be removed by magic angle spinning. Also, superconducting solenoids producing fields in the range of nine to fourteen tesla are not yet widely available.

Sample spinning at the magic angle has been used to attenuate second order quadrupolar broadening (4-11), but the narrowing is theoretically limited to a factor of about 3.6 (4). Sample spinning at angles other than the magic angle has been used; the angle producing the most narrowing depends on the asymmetry of the electric field gradient tensor (4,8,9,11). However, at angles other than the magic angle, any chemical shift anisotropy present is not efficiently narrowed. If there is more than one kind of site for the quadrupolar nucleus, then the optimum angle may be different for the different sites, leading to narrowing of only part of the NMR signal.

The selective averaging of the second order quadrupole interaction by a multiple pulse sequence has not yet been achieved. For a multiple pulse sequence to produce line narrowing, the reciprocal of the cycle time must be much greater than the width of the unnarrowed line. Since cycle times can be reduced to a few tens of microseconds, a multiple pulse sequence could be applied to lines as broad as 40 kHz, whereas sample spinning is limited by rotational periods of at least 200 μsec and is conveniently applied to lines no more than 10 kHz wide. Furthermore, provided the basic cycle time requirement is fulfilled for each different site, a multiple pulse sequence will efficiently average all the different quadrupolar couplings within a sample, unlike variable angle spinning.

The development of multiple pulse sequences has always followed the discovery of an echo that refocuses the interaction to be averaged. The Carr-Purcell-Meiboom-Gill pulse sequence for removing the effects of an inhomogeneous magnetic field is based on the spin echo, discovered by Hahn in 1950 (12). Similarly, the WAHUHA and MREV-8 pulse sequences for the selective averaging of the homonuclear dipolar interaction were based on the dipolar echo, first observed by Lowe in 1957 (13).

The intention of the work presented here was to establish the existence of an echo caused by refocusing of the second order quadrupolar interaction, and to develop a multiple pulse sequence, based on this echo, for the selective

averaging of this interaction. Such a sequence, in combination with magic angle spinning to remove chemical shift anisotropy, would provide a powerful and useful method for the study by NMR of chemical systems containing quadrupolar nuclei. Although the ultimate goals of this project were not achieved, unexpected results were obtained. An echo of problematic origin was found; its characteristics are considered interesting and will be described. In addition, the effects of a multiple pulse sequence based on this echo will be discussed.

THE QUADRUPOLAR INTERACTION

Origin and Powder Patterns

Quadrupolar effects on the magnetic resonance spectra of nuclei originate from the electrostatic interaction of a nucleus with its environment (14-17). The classical energy of interaction between a charge distribution with density ρ and an electric potential created by external sources is given by $H = \int \rho(\vec{x}) V(\vec{x}) d\vec{x}^3$. After expansion of $V(\vec{x})$ in a Taylor series about the nuclear center of mass, the only nonzero term of interest is

$$\Sigma_{ij} \; \partial^2 V/\partial x_i \partial x_j)_{\vec{x}=0} \int x_i x_j \rho d^3\vec{x} \; ,$$

in which $\partial^2 V/\partial x_i \partial x_j)_{\vec{x}=0}$ $(=V_{ij})$ represents the electric field gradient (EFG) at the nucleus, and $\int x_i x_j \rho d^3\vec{x}$ the electric quadrupole moment associated with a nonspherical charge distribution in the nucleus. Since the only significant field gradients are a result of internal fields, the interaction between the EFG and the nuclear quadrupole moment is very sensitive to details of the charge distribution around the atom. The effects of the quadrupolar interaction on the NMR of those nuclei having an electric quadupole moment (that is, those with a spin angular momentum quantum number I greater than one-half) have been utilized extensively in studies of solids. Details of theory and applications appear in reviews by Cohen and Reif (15) and Kanert and Mehring (18).

After simplification and replacement of ρ with the appropriate quantum mechanical operators, the Hamiltonian for the quadrupole interaction in the principal axis system of the electric field gradient tensor is (16,17,19)

$$H_Q = \frac{(e^2qQ)}{4I(2I-1)h}\left[3I_Z^2 - I(I+1) + \frac{\eta}{2}(I_+^2 + I_-^2)\right]$$

The principal axis system of the EFG tensor is chosen such that $|V_{ZZ}| \geq |V_{YY}| \geq |V_{XX}|$; the two parameters necessary to specify the EFG tensor are then taken to be the asymmetry parameter η, defined as $(V_{XX} - V_{YY})/V_{ZZ}$, and eq, defined as V_{ZZ}. In the presence of a sufficiently strong magnetic field (vide infra), the nuclear spin angular momentum is quantized along the direction of the field and it is more appropriate to consider the Hamiltonian in the laboratory axis system defined with the z-axis coincident with the field. In the lab axis system the Hamiltonian becomes

$$H_Q = (\nu_Q/2)\{3I_z^2\cos^2\theta + 3I_x^2\sin^2\theta + 3\sin\theta\cos\theta(I_zI_x + I_xI_z) - I(I+1) + (\eta/6)[\cos2\phi(I_y^2 - I_x^2) - \sin2\phi(I_xI_y + I_yI_x)]\}$$

where θ and ϕ are the polar angles describing V_{ZZ} relative to the z-axis and ν_Q is defined as $3e^2qQ/2I(2I-1)h$.

In a sufficiently strong magnetic field, B_0, defined by the condition $\gamma B_0 >> e^2qQ/2I(2I-1)$, the quadrupolar interaction can be treated as a perturbation on the Zeeman interaction. The Zeeman Hamiltonian (in units of rad/sec) is given by $H_Z = -\gamma B_0 I_Z$ and creates $2I+1$ equispaced energy levels with eigenvalues $E_m^{(0)} = -\gamma B_0 m$. Magnetic dipole

transitions induced by a radio frequency field perpendicular to B are restricted by the selection rule $\Delta m = \pm 1$, leading to 2I superimposed transitions of frequency $\nu(m \leftrightarrow m-1) = \gamma B_0/2\pi = \nu_L$ (Figure 1a). To first order, the effect of the quadrupole interaction is to shift the transition frequencies by $\nu^{(1)}$ (Figure 1b and Table 1). The central transition ($1/2 \leftrightarrow -1/2$) remains unaffected by the perturbation to first order. The additional effect of the second order correction $\nu^{(2)}$ shifts not only the satellite transitions (each transition in the pair $\pm m \leftrightarrow \pm m-1$ shifts the same way) but also the central transition (Figure 1c and Table 1) (20).

For polycrystalline or amorphous samples, all possible orientations of the EFG tensor with respect to B_0 are found. The superposition of lines throughout the range of frequencies produced by the random variation of θ and ϕ creates a characteristic powder pattern; examples are shown in Figure 2. Regardless of the value of I, the separation between the innermost divergences is given by ν_Q when $\eta = 0$. Values of e^2qQ are conveniently obtained from ν_Q (Table 1). Second order effects of the quadrupolar perturbation lead to powder patterns for the central transition; the form depends only on η and not on I (Figure 3) (21). The values of e^2qQ, η and ν_L are frequently obtainable from the powder pattern of the central transition (Table 1). In actual practice, dipolar broadening blunts the sharp singularities in the powder patterns. When there is a broad distribution in ν_Q throughout the sample, the features that originate from satellite

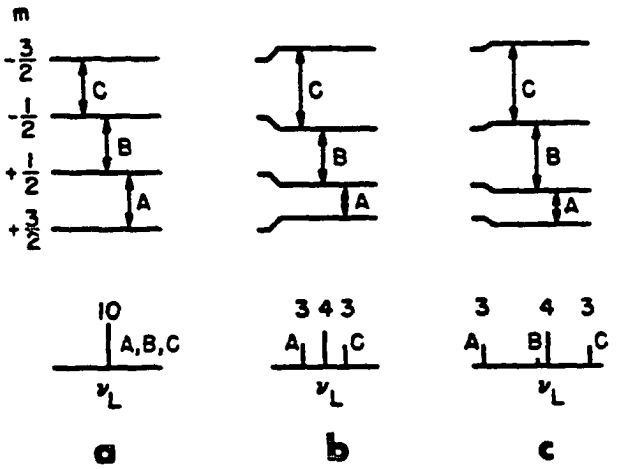

Figure 1. Energy levels and theoretical NMR spectra for a nucleus with I = 3/2, with a) $\nu_Q = 0$, b) $\nu_Q \neq 0$, first order correction, and c) $\nu_Q \neq 0$, second order correction (15).

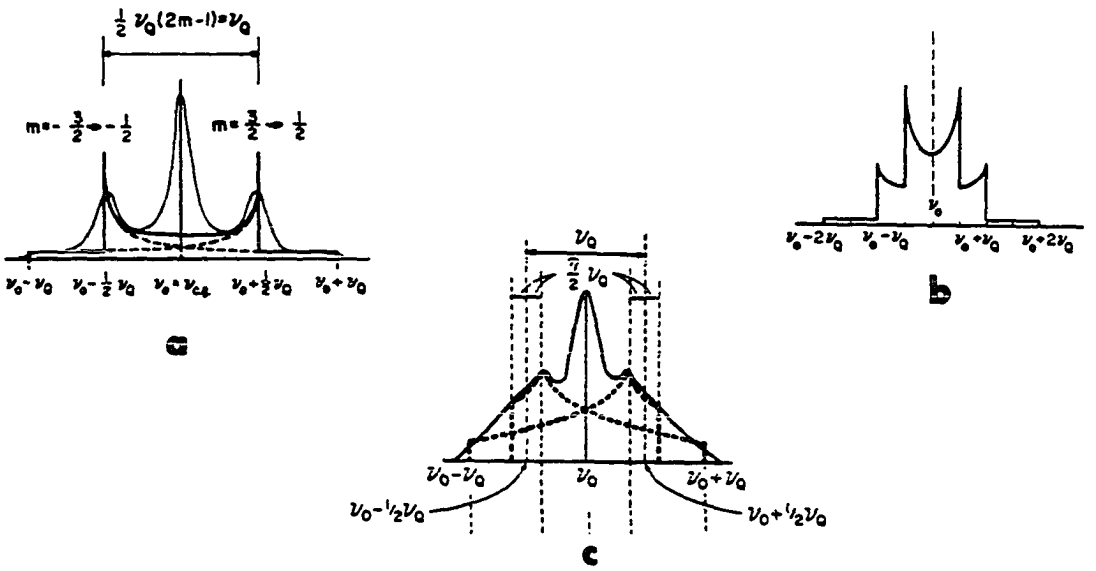

Figure 2. Powder patterns showing the first order effects of the quadrupole interaction for a) I = 3/2, $\eta = 0$, b) I = 5/2, $\eta = 0$, and c) I = 3/2, $\eta \neq 0$, with dipolar broadening (21).

transitions frequently become invisible; in effect, the width of each of the peaks whose superposition creates the powder pattern is proportional to |m| (22). Thus in many samples only the powder pattern of the central transition is observable.

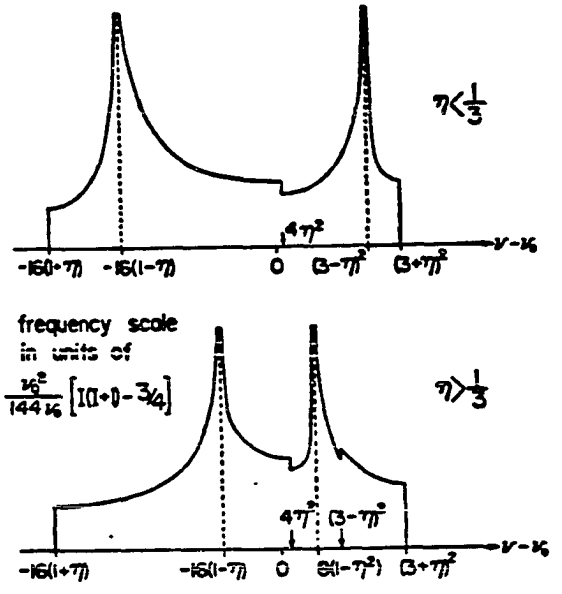

Figure 3. Powder pattern showing the second order effects of the quadrupolar interaction on the central transi-transition of nuclei with non-integral spin (23).

Table 1. Expressions for Some Quantities Associated with the Quadrupolar Interaction

---

splitting between innermost divergences in first order powder pattern: $\nu_Q = (1 - \eta)(3e^2qQ)/[2I(2I-1)h]$

first order correction to transition frequencies:

$$\nu^{(1)} = \nu_Q(h/4)(m - 1/2)(3\cos^2\theta - 1 - \eta\sin^2\theta\cos2\phi) .$$

second order correction to transition frequencies:

$$\nu^{(2)} = (\nu_Q^2/12\nu_L)\{(3/2)\sin^2\theta[(A+B)\cos^2\theta - B] + \eta\cos2\phi\sin^2\theta[(A+B)\cos^2\theta + B] + (\eta^2/6)[A - (A+4B)\cos^2\theta - (A+B)\cos^2 2\phi(\cos^2\theta-1)^2]\},$$

where

$$A = 24m(m-1)-4I(I+1)+9 \quad \text{and} \quad B = (1/4)[6m(m-1)-2I(I+1)+3$$

splitting between the divergences in second order powder pattern of central transition:

$$\Delta\nu = (\nu_Q^2/144\nu_L)[I(I+1) - (3/4)](\eta^2 + 22\eta + 25)$$

shift in center of gravity of powder pattern of central transition from unperturbed frequency ν_L:

$$\nu_L - \nu_{cg} = (\nu_Q^2/120\nu_L)(2I-1)(2I+3) \quad \text{for } \eta = 0$$

Spin Dynamics

Depending on the ratio ν_{rf}/ν_Q, the rate of precession in an rf field of the magnetization associated with a system of quadrupolar nuclei ranges from γB_{rf} to $(I + 1/2)\gamma B_{rf}$ (16,24 25). The minimum precession rate, γB_{rf}, occurs in the case where $\nu_{rf}/\nu_Q >> 1$, referred to as non-selective excitation since all transitions are induced. The maximum precession rate occurs for selective excitation of the central transition, where $\nu_{rf}/\nu_Q << 1$. The precession rate for selective excitation of any transition $m \leftrightarrow (m+1)$ is given by $[(I-m)(I+m-1)]^{1/2}$; for the satellite transitions the precession rate is less than that for the central transition. Values of ν_{rf}/ν_Q between these two extremes result in intermediate precession frequencies. Fenzke et al. (25) report precession rates (in the form of graphs of the intensity of the central peak of a spin 5/2 versus pulse length) for intermediate values of ν_{rf}/ν_Q.

The spin dynamics of quadrupolar nuclei allow the use of a simple one-pulse two-dimensional experiment for the determination of quadrupolar parameters characteristic of the system (26,27). The free induction decays recorded after successively longer pulses are Fourier transformed two-dimensionally, with respect to the time over which the free induction decay is recorded and with respect to the pulse length. Since the initial intensity of the free induction decay is modulated by the extent to which the magnetization has been rotated by the pulse, the Fourier transform with respect to

the pulse length gives a signal at a frequency corresponding to the precession frequency of the magnetization in the rf field. Projections of the two-dimensional display onto the axis representing precession frequency can be used to infer ν_Q and η (26). The two-dimensional display has been used to determine whether or not the central transition is being selectively excited by observing whether the precession frequency of the magnetization is given by γB_{rf} or $(I + 1/2)\gamma B_{rf}$ (28,29). The two-dimensional experiment is most conveniently carried out on-resonance with quadrature detection. With single phase detection, off-resonance effects complicate the results by introducing a shift in the position of the signal along the axis representing precession frequency (30).

Echoes

An important phenomenon in the NMR of nuclei with $I > 1/2$ is the quadrupolar echo. Assuming that $\nu_{rf} >> \nu_Q$, $\eta = 0$ and $I = 5/2$, if a β_ϕ pulse is applied to a system of quadrupolar nuclei at a time τ (for $\tau < T_2$) after a 90°_ϕ preparation pulse, "echoes" will occur at times $(3/2)\tau$, 2τ and 3τ after the preparation pulse, with maximum amplitude for $\beta_\phi \sim 35°$ (31). The echoes result from a rephasing (or refocusing) of the NMR signals from the satellite transitions; the number of echoes that appear depends on I. If relaxation effects and the second order perturbation by the quadrupolar interaction are ignored, then the signal from the central transition is a

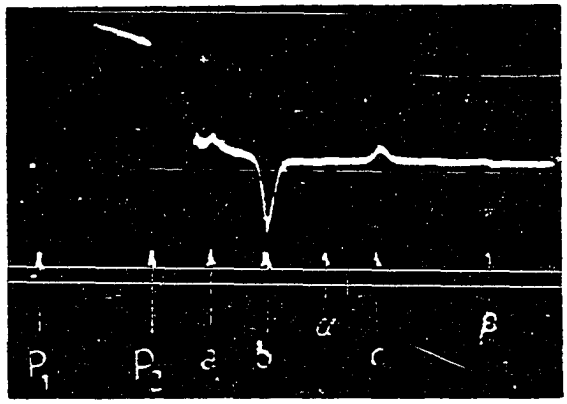

Figure 4. The quadrupolar echoes from a single crystal of KI, for $\beta = 35°$. Allowed echoes are denoted by a, b, and c; forbidden echoes are denoted by α and β (31).

constant (but not the same) before and after the refocusing pulse, and the echoes are superimposed on this signal. Changing the phase of the β_ϕ pulse to $\phi + 90°$ increases the amplitude of the allowed echoes (32,33). When ν_Q is a significant fraction of ν_{rf}, additional echoes originating from the forbidden transitions $\Delta m = \pm 2$ occur at times $(5/2)\tau$ and 4τ after the preparation pulse. An example is shown in Figure 4.

The utility of the quadrupolar echo comes from the fact that the shape of the allowed echoes is related to the Fourier transform of the distribution of ν_Q throughout the sample (31). Thus the inverse of the width of the echo is a measure of the range of crystalline defects. This information is obtained most directly from the $(3/2)\tau$ and 3τ echoes created by a $\beta_{\phi+90°}$ refocusing pulse (33). The quadrupolar echo is also useful in that the limitations of receiver dead time can be circumvented by recording the free induction decay begin-

ning at the center of the echo, thus reducing the distortion of very wide lines (34,35).

For a wide range of solids, both magnetic effects (a distribution in Zeeman frequencies $\delta\nu_L$) and quadrupolar effects occur. In these systems, a β_ϕ pulse applied at a time τ after a 90°_ϕ preparation pulse creates an echo only at a time 2τ after the preparation pulse, assuming that ν_{rf} is greater than both ν_Q and the variation in $\delta\nu_L$ (36). The other echoes found in purely quadrupolar systems are suppressed by the magnetic effects. The variation of the amplitude of this hybrid echo with β differs from that found from either the magnetic or quadrupolar perturbations alone; experimental observation of this variation may allow one to determine whether magnetic, quadrupolar or the combined effects are present. The amplitude of the hybrid echo becomes zero for $\beta = 180°$, where the amplitude of the contribution from magnetic effects (the Hahn echo (12)) is a maximum. Thus the distribution of magnetic effects can be distinguished from quadrupolar effects. A similar direct separation of quadrupolar effects from magnetic effects is not possible. Comparison of the hybrid and Hahn echoes has been used to determine the distribution of electric field gradients in aluminum particles (37,38). In a system with a single quadrupole coupling and a distribution in Zeeman energies, the amplitude of the echo produced by 90°_ϕ-τ-β_ϕ is modulated as a function of τ; the frequency of modulation is related to the quadrupole coupling (39).

The additional effects of dipolar interactions have also been considered. The expression describing an echo at time 2τ produced by 90°_ϕ-τ-β_ϕ can be divided into four parts, each with a characteristic plot of echo amplitude versus β and arising from a particular combination of effects and transitions (40). In principle it is possible to separate the effects of the different interactions. Again, the development accounted for only first order quadrupolar perturbations with an axially symmetric EFG tensor (η=0) and assumed $\nu_{rf} >> \nu_Q$. For selective excitation ($\nu_Q >> \nu_{rf}$) of the central transition, a 90°_ϕ-τ-90°_ϕ sequence has been shown to create an echo (41). The echo is due entirely to the quadrupole interaction, but cannot directly give any information about the interaction.

EXPERIMENTAL

Adjustment of Pulse Widths

A common practice in Fourier transform NMR is to adjust the rf pulse to give a flip angle of 90° in order to obtain the maximum signal when recording a simple free induction decay. In the application of FT-NMR to solids, it is convenient to make this pulse length adjustment while observing a liquid sample of the same nucleus. The use of a liquid or solution has the advantage of a longer free induction decay and frequently a greater signal.

For spin-1/2 nuclei, the 90° pulse length is the same for both solids and liquids. However, for quadrupolar nuclei, the pulse length that rotates the observed magnetization by ninety degrees is usually different for solids and liquids. In solids with a strong quadrupole coupling, a routine experiment may only succeed in exciting the central transition. In this case, the magnetization precesses in the rf field of the pulse at a rate equal to $(I+1/2)\gamma H_{rf}$ (16). For a spin-5/2 system, then, the precession rate is three times faster than it would be if the same nuclei were in a liquid, and the length of a 90° pulse is one-third the length of the corresponding pulse in a liquid. Thus if a 90° pulse for the solid is to be adjusted using a liquid, it is necessary to be able to adjust pulse lengths to something other than 90° when observing the liquid.

A convenient way of adjusting pulse lengths is to observe the response of a liquid sample to a string of β_ϕ pulses 200 μsec apart, with phase detection at ϕ+90° (42). In terms of the classical picture of a magnetization vector $\vec{M}_o$ in a frame rotating at the Larmor frequency, if ϕ = 90° the first pulse will rotate $\vec{M}_o$ from its equilibrium position along the z-axis to a position in the xy-plane, where the detected signal is a maximum, $|\vec{M}_o|$. The second pulse will rotate $\vec{M}_o$ further to the -z-axis, where the detected signal is zero. Similarly, the third pulse will rotate $\vec{M}_o$ to a position in the xy-plane opposite to its position after the first pulse, and the signal will now be a maximum in the negative direction. Thus a sequence of many pulses will result in a pattern of +, 0, -, 0, ... (Figure 5a).

The same pulse sequence will also result in distinctive patterns when β = 60° or 45°. The first 60° pulse will rotate $\vec{M}_o$ such that the signal detected will be $|\vec{M}_o|\sin 60°$. The second 60° rotation will result in the same projection of $\vec{M}_o$ onto the xy-plane and thus the same signal, while the third 60° rotation will bring $\vec{M}_o$ to the -z-axis, where the signal will be zero. Thus the pattern for β = 60° will be +, +, 0, -, -, 0 ... (Figure 5b). When β = 45°, the pattern will be +, ++, +, 0, -, --, -, 0 ... (Figure 5c), where + represents $|\vec{M}_o|\sin 45°$ and ++ represents $|\vec{M}_o|$. Because each of these tuning patterns is so distinctive when viewed over the entire length of the decay, it is convenient and more accurate to adjust the pulse length while looking for

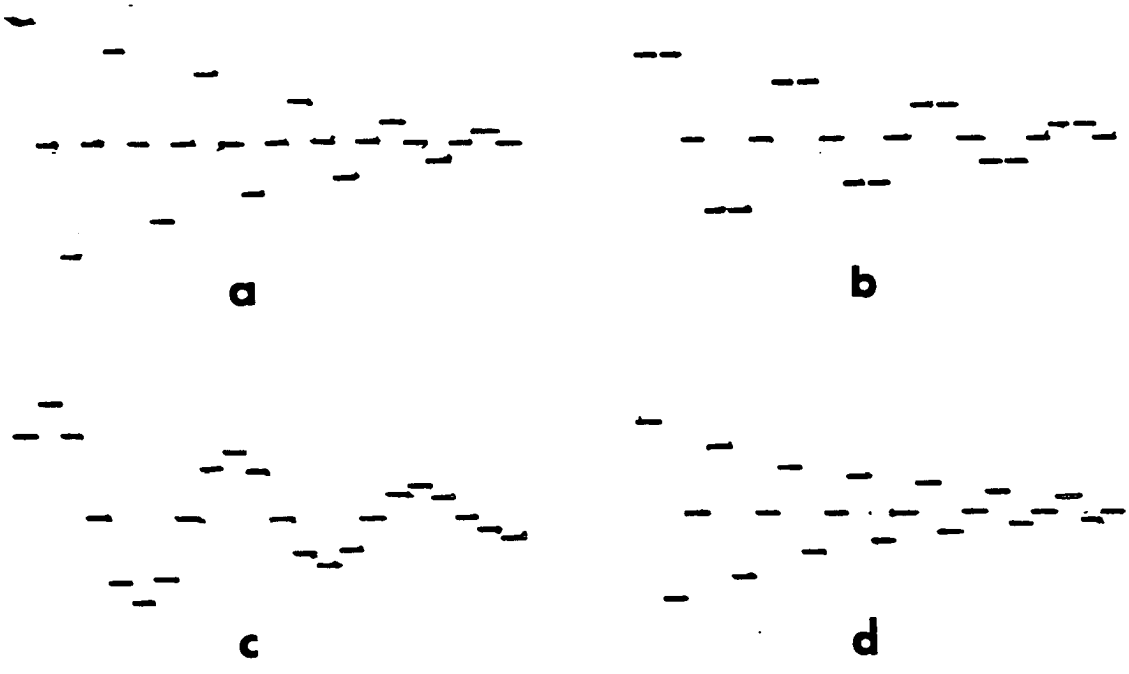

Figure 5. Tuning patterns for $(\beta_\phi\text{-}\tau\text{-})_n$, where β = a) 90°, b) 60°, c) 45° and d) 120°.

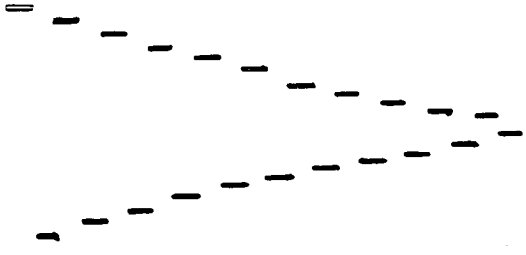

Figure 6. Tuning pattern for $90^\circ_x\text{-}(\tau\text{-}180^\circ_z)_n$.

the pattern as a whole rather than just the results of the first few rotations.

In general, for a 180°/n flip angle, the pattern will be one in which the magnetization after every n^{th} pulse is zero. When n > 4, the patterns are no longer as distinctive as the ones described above, and from a practical standpoint it is necessary to adjust the flip angle by changing the pulse width until the n^{th} rotation gives zero signal. For greater accuracy it is possible to make the $2n^{th}$ and $3n^{th}$ rotations also give zero signal, but it is difficult to make the $4n^{th}$ and greater rotations give zero signal while still keeping the $3n^{th}$ and smaller at zero.

Finally, distinctive patterns also result for $\beta = 120°$ and 180°. From the classical vector picture it is clear that for $\beta = 120°$ the pattern is +, −, 0 ... (Figure 5d), and for $\beta = 180°$ simply 0, 0, 0 ... Pulses having flip angles between 90° and 180° are frequently necessary for the formation of echoes.

In the context of the present study, one more tuning pattern is important. Again thinking in terms of the classical picture of a magnetization vector in the rotating frame, the response of $\vec{M}$ to a rotation of 180° about the z-axis is a shift in phase by 180°. Thus the pattern resulting from a succession of 180°_{z} pulses after an initial β_{ϕ} pulse is +, − ... as displayed in Figure 6.

Determination of Spin Dynamics

Depending on the relative strengths of the rf field and the quadrupole coupling, the pulse length that will rotate the observed magnetization of an $I > 1/2$ system by 90° will vary (25). When the pulse is applied at the Larmor frequency of the central transition, the precession rate of the magnetization in the rf field of the pulse can range from γH_{rf} to $(I+1/2)\gamma H_{rf}$. In the case where $\omega_{rf} << \omega_Q$, only the central transition is being excited ("selective excitation"), and the precession rate will be $(I+1/2)\gamma H_{rf}$. When $\omega_{rf} >> \omega_Q$, all transitions are excited ("nonselective excitation") and the precession rate will be γH_{rf}. For (ω_{rf},ω_Q) between these extremes, the precession will be at an intermediate rate. Applying the rf pulse off-resonance complicates this picture of the precession rate.

In order to determine what degree of excitation is being achieved for a given sample and rf field, the precession rate of the observed magnetization can be monitored by finding what pulse length gives a flip angle of 90°. This pulse length can be related to the extreme of nonselective excitation by comparison with the pulse length that gives a 90° flip angle for a solution or liquid of the same nucleus. Since the size of the NMR signal depends on the projection of the magnetization onto the xy-plane, it is convenient to infer the flip angle by observing the amplitude of the free induction decay as the pulse length is varied.

Rather than measuring pulse lengths by direct observation with an oscilloscope, pulse lengths were expressed as the corresponding flip angle for an aqueous solution of aluminum. Utilizing the tuning patterns described earlier, the dial setting for pulse length on the pulse program generator was recorded as a function of flip angle. The results were fit to a line with the linear regression feature of a TI-55 or HP-25 calculator. The amplitude of the free induction decay from the solid sample was measured for many different dial settings in the neighborhood of both 90° and 180° flip angles. Using the line determined from the solution, the dial setting that gave the maximum signal was converted to a flip angle. For aluminum, with I = 5/2, nonselective excitation corresponds to a 90° flip angle for the solution and selective excitation of the central transition corresponds to a 30° flip angle for the solution.

The amplitude of the free induction decay for the solids was determined by the size of the first full oscillation in the off-resonance free induction decay. Unfortunately, this method of measuring the size of the signal introduces a distortion into the results because of the poorly understood influence of the resonant offset on the spin dynamics of the quadrupolar nuclei.

180°_{z} Pulses

In early experiments, 180° rotations about the z-axis were accomplished using a dc pulse through a Helmholtz coil

aligned with the direction of the static magnetic field. The dc pulses were generated by a pulsed field gradient unit constructed in the Ames Laboratory. Pulse lengths were controlled by a thumbwheel switch on the front panel and could be adjusted in 10 μsec increments. The output current was continuously variable from 0 to 50 amps, and the pulse rise time was set to the shortest possible value, about 0.5 μsec per amp. The pulses were triggered by a "T1" pulse from the pulse program generator through CNTRL-bar on the back panel, and the field gradient unit was driven by a 1 MHz signal from the pulse program generator.

The first design for a z-coil in the NMR probe is shown in Figure 7a. Both sections of the Helmholtz coil have 8 turns at a pitch of 14 turns per inch. The two sections are separated by about 8 mm, and the coil is wound on an 8 mm diameter Teflon rod into which 1 mm deep square grooves have been machined to hold the coil in place. The wire is 20 AWG Armored Polythermaleze. With this design, a 100 μsec pulse at 37 amps gave a 180°_{z} tuning pattern lasting only 500 μsec for an aqueous solution of aluminum.

Ideally, the pulse should be as short as possible and the magnetic field in the z-coil should be as homogeneous as possible. To approximate delta function pulses, the pulse lengths applied to typical solid samples need to be only a few microseconds long. If the homogeneity of the field in the z-coil is poor, then only a small portion of the sample will experience pulses of the proper length and the net

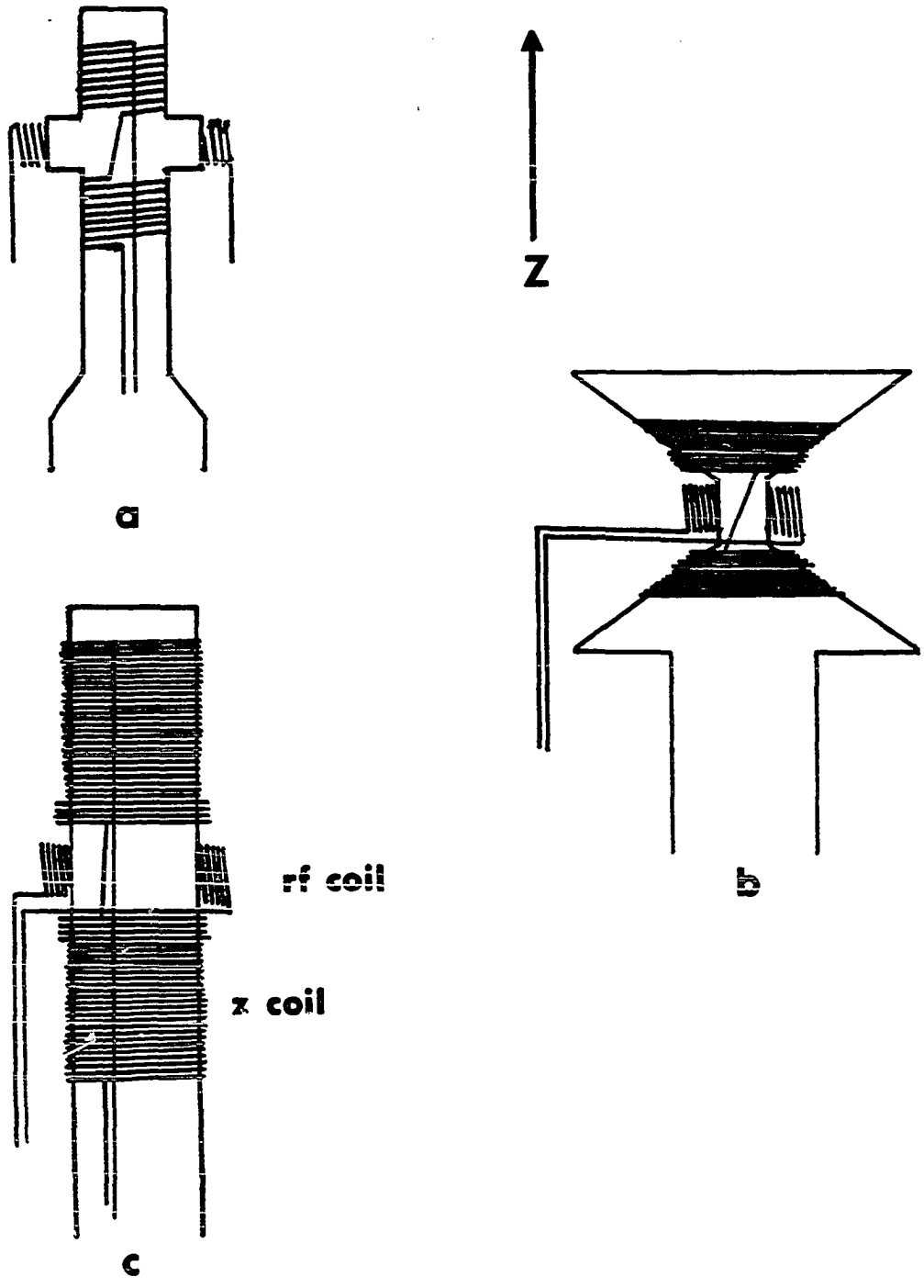

Figure 7. Three configurations for producing z-pulses with a dc current through a coil aligned along the z-axis.

signal will disappear more rapidly than expected due to less efficient rephasing. With a z-coil having a high degree of homogeneity, the tuning pattern should last as long as the simple free induction decay of the aqueous aluminum, about 5 msec.

In order to improve the homogeneity of the magnetic field in the z-coil, the second design called for each section of the Helmholtz coil to be wound about a Teflon cone tapering at an angle of 54° toward the z-axis, with a width at the narrowest part of 5 mm, as in Figure 7b. The windings were as close as possible and secured to the Teflon cone by epoxy. A 60 μsec pulse at 40 amps gave a 180°_{z} tuning pattern for aqueous aluminum, with a decay lasting about 1.6 msec.

In the final design, a 12.5 mm Teflon rod supported a Helmholtz coil in which each section was about 2 cm long and was wound as closely as possible with four overwindings near the rf coil, as in Figure 7c. With this configuration, a second high impedance resonance appeared in the rf circuit a few MHz below the desired resonance. A half-inch wide ground braid wrapped around the lower part of the z-coil and secured with a nut and bolt removed this undesired resonance. A 180°_{z} tuning pattern for aqueous aluminum was obtained with an 80 μsec pulse at 31 amps. This design gave the best z-coil homogeneity with a tuning pattern lasting about 2 msec.

Since rf pulses originate in a tuned resonant circuit, which stores energy more efficiently than a nonresonant Helmholtz coil, rf pulses can be made shorter than dc pulses.

Consequently, all but a few initial experiments used a composite rf pulse to generate a 180° rotation around the z-axis.

The composite rf pulse used most often was 90°_{-x}-180°_{y}-90°_{x}, where each pulse begins as soon as possible after the preceding pulse. This composite pulse is of the general form 90°_{-x}-θ-90°_{x}, which has the effect of a rotation by θ about the z-axis (43). The timing of the composite pulse was adjusted by observing the transmitter output on the oscilloscope with the most sensitive vertical scale possible and adjusting the delays to be as small as possible without the visible portion of the pulse ringdown overlapping with the following pulse. When observed on an insensitive vertical scale, the separation between pulses was usually ~0.2 μsec.

Another composite pulse that produces a 180° rotation about the z-axis is 180°_{x}-180°_{y}. Since one of the four possible pulse channels must be tuned to something other than 180° for a preparation pulse, this form of composite pulse has the disadvantage that it does not allow the invert feature of this laboratory's NMR spectrometer to be used. If one of the 180° pulses was constructed of two back to back 90° pulses, the invert could be used, but the pulse program generator/rf unit fails to produce a good pulse if the pulse immediately preceding it is of the same phase. The best results were obtained using the 90°_{-x}-180°_{y}-90°_{x} composite pulse.

RESULTS AND DISCUSSION

An NMR echo has been observed that was initially believed to be due to refocusing of the second order quadrupolar broadening of the central transition of ^{27}Al nuclei (44). When a 180°_{z} pulse was applied at a time τ after a 90°_{x} preparation pulse, an echo was seen at a time 2τ after the initial pulse. Examples of this echo are shown in Figure 8. Using average Hamiltonian theory, it was found that the application of this pulse sequence to the second order quadrupolar interaction, as represented by the spin operator $(I_zI_x+I_xI_z)$, would cause the first term in the Magnus expansion to be zero. Thus, at time 2τ, the second order effects of the quadrupolar interaction would appear to be nonexistent. However, subsequent consideration of the phenomenon has led to the conclusion that this interpretation of the echo is incorrect. There are two mistakes in the analysis on which the initial interpretation was based.

In the laboratory frame of reference, the Hamiltonian describing the quadrupolar interaction for the case of an axially symmetric electric field gradient is given by (16,19)

$$H_Q \propto [3I_z^2\cos^2\theta + 3I_x^2\sin^2\theta + 3(I_zI_x+I_xI_z)\sin\theta\cos\theta - I^2].$$

The following expression for the second order correction to the stationary state energies $E_m^{(o)}$ is a well-known result from Rayleigh-Schroedinger perturbation theory:

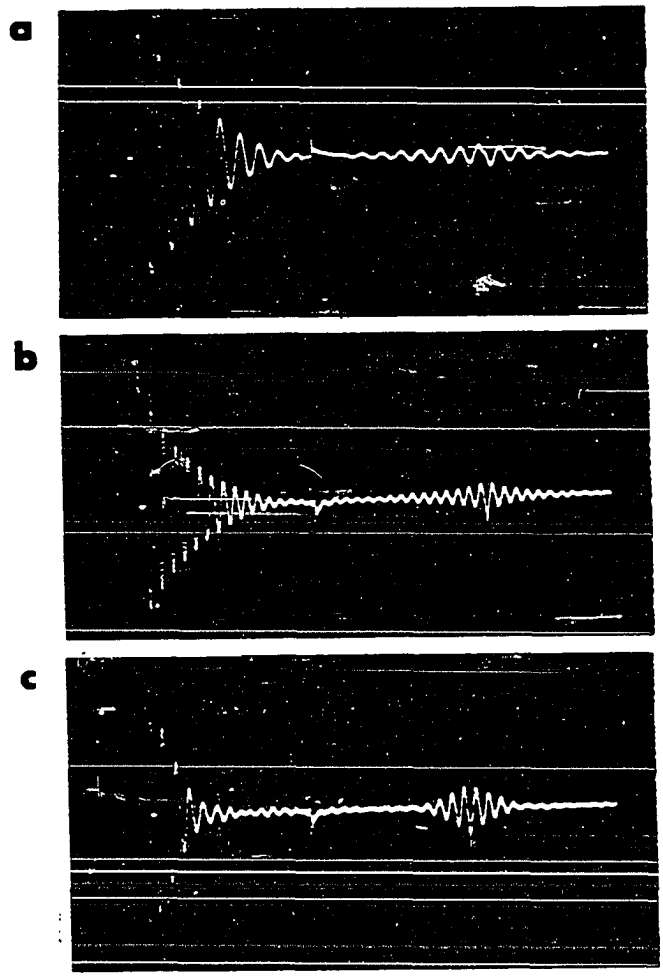

Figure 8. Echoes formed by a 180°_{z} refocusing pulse applied after the free induction decay following a 90°_{x} preparation pulse; a) α-alumina, b) jadeite, and c) soda feldspar (41).

$$E_m^{(2)}{}_{(m\neq n)} = \Sigma_n |\langle In|H^P|Im\rangle|^2 / (E_m^{(0)} - E_n^{(0)}).$$

Here the unperturbed states are the Zeeman states and the perturbation is the quadrupolar interaction. The term in H_Q proportional to I_x^2 contributes to $E_m^{(2)}$ as well as the term proportional to the anticommutator $[I_z,I_x]^+$, but this $I_x{}^2$ term was neglected in the initial analysis.

Furthermore, a difficulty arises because the Hamiltonian to be averaged does not commute with the Zeeman Hamiltonian. If the problem is considered in the rotating frame, the non-secular parts of H_Q, given by I_x^2 and $[I_z,I_x]^+$, become time dependent; I_x is replaced by $(I_x\cos\omega_o t - I_y\sin\omega_o t)$, where ω_o is the Larmor frequency. The application of average Hamiltonian theory to this problem does not yield a simple result that obviously predicts the formation of an echo. In the initial analysis, the spin operator dependence of the second order quadrupolar interaction was incorrectly taken to be $[I_z,I_x]^+$ in the rotating frame, and thus an inappropriate result was obtained.

The refocusing pulse used to observe the reported echo was a composite radiofrequency pulse of the form 90°_{-x}-180°_{y}-90°_{x}, which has the effect of a 180° rotation about the direction of the static magnetic field (z-axis) (43). The same rotation can also be achieved by applying a dc pulse to a Helmholtz coil aligned along the z-axis. This approach was used successfully to generate 180°_z pulses but was not applied successfully to solid samples. Since rf pulses originate in

tuned resonant circuits, which store energy more efficiently than a nonresonant Helmholtz coil, rf pulses can be made shorter than dc pulses and for this reason the composite rf pulse was utilized.

Although the initial interpretation of the echo generated by a composite 180°_{z} pulse appears incorrect, the echoes reported are an interesting result. The following experimental observations are described for the purpose of providing an empirical characterization of the echoes after a composite 180°_{z} pulse. The experiments were conducted on the ^{27}Al resonances of powdered samples of α-alumina (α-Al_2O_3) and ordered albite ($NaAlSi_3O_8$). Both compounds contain only a single kind of aluminum. In each case dipolar interactions are small relative to the observed linewidth of approximately 8 kHz, which is believed to be mostly due to broadening by the second order effects of the quadrupolar interaction.

In order to determine the proper pulse lengths for the flip angles 90° and 180°, a study of the amplitude of the free induction decay versus pulse length was performed. Results similar to those reported by Fenzke et al. were obtained (25). For example, the powdered sample of ordered albite was found to have a 90° pulse length corresponding to a 34° flip angle for $Al(H_2O)^{3+}$, and a 180° pulse length corresponding to an 84° flip angle for $Al(H_2O)^{3+}$. Initially, selective excitation of the central transition was assumed and the pulse lengths were adjusted to correspond to

30° and 60° for $Al(H_2O)^{3+}$. The quality of the echoes did not depend on which set of pulse lengths was utilized.

The amplitude of the echo generated by a $180°_z$ pulse was strongly dependent on the resonance offset, and was smaller than the amplitude of the echo generated by either a simple $90°_y$ or $180°_y$ pulse. On some occasions the $180°_z$ echoes seemed to be out of phase, that is, the phase of the free induction decay at the center of the echo was something other than 0° or 180° (Figure 9). When the $180°_y$ pulse was removed from the composite pulse while still retaining the delay (usually ~1 μsec) between the 90_{-x} and 90_x pulses, the size of the echo increased by as much as a factor of four, depending on resonance offset. On the other hand, removing the delay as well as the $180°_y$ pulse caused the echo to disappear, as expected from a classical picture of the effect of a $90°_{-x}$-$90°_x$ composite pulse on a spin-1/2 system.

When a train of echoes created by composite $180°_z$ pulses was observed, the amplitudes of the echo centers traced out an oddly shaped envelope, in which the first few echoes (the number depending on the time between echoes) increased in amplitude before an apparently exponential decay in echo height appeared (Figure 10). In addition, this exponential decay did not seem to connect with the initial amplitude of the free induction decay after the preparation pulse. In the case of albite, the decay traced out by the echo centers had a time constant of about 4 msec. For comparison, the T_1 for this sample was about 2 sec and the T_2^* was about 200 μsec.

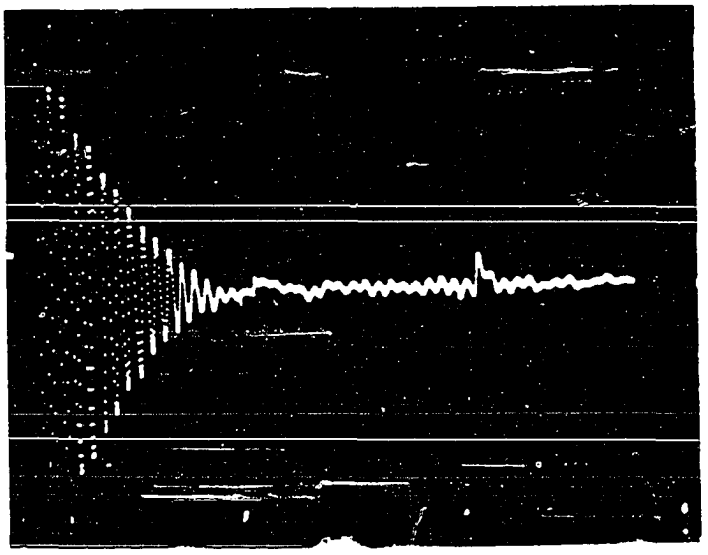

Figure 9. An echo generated by a 180°_{z} refocusing pulse appearing to be out of phase.

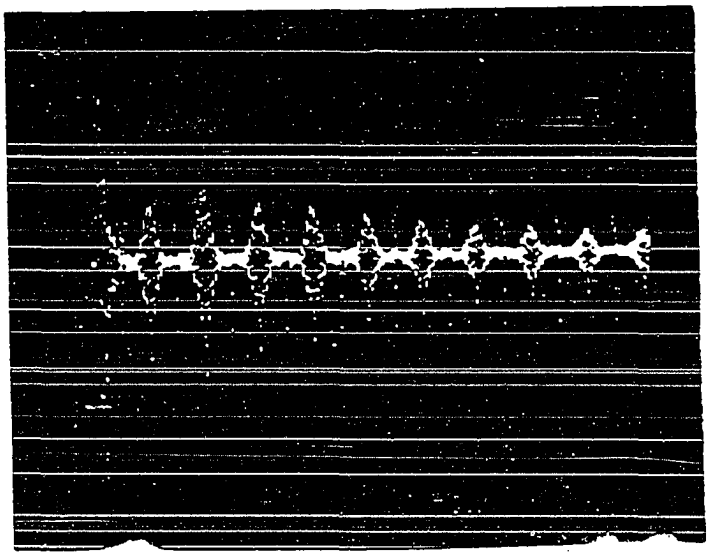

Figure 10. A train of echoes generated by 180°_{z} refocusing pulses, showing the unexpected shape of the envelope traced out by the centers of the echoes.

In the context of the initial interpretation of the echo formed by a 180°_{z} composite pulse, it was noted that if a train of 180°_{z} pulses is applied to the sample and the magnetization in the windows between the pulses is observed stroboscopically, the effects of the second order quadrupole interaction would be removed from the resulting signal but the chemical shift interaction would be unaffected. Since the chemical shift interaction should be unaffected by this pulse sequence, the Fourier transform of the signal should yield a spectrum with enhanced resolution due to removal of broadening by the second order quadrupolar interaction. As described above, the initial interpretation of the echo was incorrect and the prediction that a multiple pulse sequence based on a train of 180°_{z} pulses will selectively average the second order quadrupolar interaction can no longer be supported. However, the prediction that the chemical shift interaction will be unaffected would seem to be still valid. Surprisingly then, the application of this pulse sequence to albite lengthened the time decay from 200 μsec to 4 msec, but the decay showed no oscillation regardless of the resonance offset. Thus, contrary to expectation, the chemical shift interaction is being averaged by the pulse sequence, and it is unknown at this point whether or not there is any averaging of the second order quadrupolar interaction.

Since interference of the satellite transitions with the central transition could possibly cause the failure of the multiple pulse experiment, a single crystal of albite was

studied. The inner pair of satellite transitions was easily observable and appeared 189 kHz away from the central transition with the crystal in a definite (but uncharacterized) orientation. The satellite peaks were successfully eliminated by using a soft preparation pulse (5.3 μsec long) to selectively excite only the central transition. The removal of the second order quadrupolar interaction by the multiple pulse sequence would result in a downfield shift in the position of the central transition. If part of the 1.5 kHz linewidth of the central transition is caused by a distribution of quadrupole couplings, then the central transition would also be narrowed by the multiple pulse sequence. Studies of the spin dynamics of the single crystal of albite indicated the expected result, namely, that a 30° pulse for a liquid rotated the magnetization associated with the central transition by ~90°.

First, the echoes created by soft preparation and refocusing pulses were observed. Experimentally, this was accomplished simply by attenuating the transmitter output until a 5.3 μsec pulse gave a flip angle of 30° for a liquid sample. The amplitude of the echo observed for an on-resonance free induction decay (with the refocusing pulse placed after the apparent end of the decay) was ~$1/8^{th}$ the initial amplitude of the free induction decay (fid). At 20 kHz off-resonance, the echo amplitude was ~1/2 that of the fid.

When a train of soft 180°_{z} pulses was applied after an on-resonance soft preparation pulse, the 180°_{z} pulses

occurring before the end of the initial fid changed the phase of the fid by 180°. This behavior is expected from a consideration of the classical picture of a magnetization vector (for I=1/2) rotated by 180° about the z-axis in the rotating frame. Superimposed on each portion of the phase-alternated fid was a small echo (Figures 11a,b). Those 180°_{z} pulses applied after the initial fid created a train of echoes, all of the same phase and superimposed on a flat baseline. With stroboscopic observation in the windows between the refocusing pulses, the points recorded after the initial fid show nothing distinguishable from baseline noise (Figure 11c); the points falling within the duration of the initial fid reflect the phase alternating effect of the 180° rotations about the z-axis.

The echo train was observed stroboscopically with a resonance offset in order to determine whether or not the pulse sequence had any effect on the second order quadrupolar interaction. The results for three different offsets are shown in Table 2. A simple fid lasts for 550 μsec, so the stroboscopically observed fid under the train of 180°_{z} pulses is longer for the two larger offsets and is shorter for the smallest offset. The offset is also affected by the pulse sequence, but in a rather erratic way.

The use of hard (~2 μsec) refocusing pulses after a soft preparation pulse gave distinctly different results. This was accomplished by turning on a gated attenuator only during

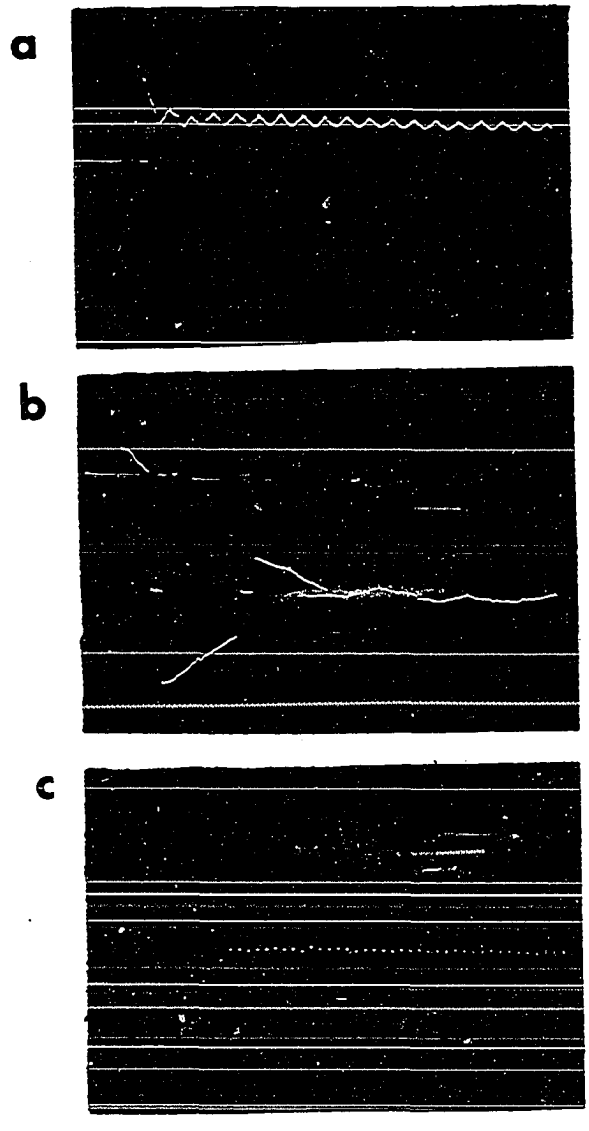

Figure 11. Echo train observed by repeated application of soft 180°_{z} refocusing pulses after a single soft 90°_{x} preparation pulse; a) 4 msec long view; b) first 1 msec of the train, with less sensitive vertical scale; c) with stroboscopic observation every 47 μsec.

Table 2. Results of Stroboscopic Observation of a Train of 180°_{z} Pulses Applied Off-Resonance to the Central Transition of a Single Crystal of Albite

Resonance offset (kHz)	offset of peak from carrier (kHz)	length of fid (μsec)
+1	0.7	~380
+4	1.7	~700
+6	4.7	~700

the preparation pulse. The amplitude of the echo created by a hard 180°_{z} pulse applied after the end of an on-resonance fid was ~$1/7^{th}$ the initial amplitude of the fid. For a resonance offset of +30 kHz, the relative amplitudes were the same as for the case of no offset. When a train of hard 180°_{z} pulses was applied to the on-resonance fid produced by a soft preparation pulse, the refocusing pulses occurring before the end of the fid changed the phase of the fid by something other than 180°, with a hint of an echo superimposed on the altered portion of the initial fid. The refocusing pulses applied after the end of the initial fid caused the formation of a train of echoes. Stroboscopic observation resulted in a long on-resonance decay regardless of the resonance offset.

It is perhaps surprising that the effect of having the refocusing pulse hard instead of soft is so distinct. The soft preparation pulse leaves the satellite transitions unaffected, but the hard refocusing pulse apparently affects them even though they are far off-resonance. The effect of the satellite transitions may be an indication that they must

be explicitly taken into account in any accurate analysis of the echoes after 180°_{z} composite pulses.

When both the preparation and refocusing pulses are hard, the characteristics of the echoes were similar to those found when the preparation pulse was soft and the refocusing pulse was hard. The major difference occurred with stroboscopic observation in the windows between pulses in a pulse train; no signal was observed either on or off-resonance.

Because of the unexpected response of spin-5/2 systems to a 180°_{z} refocusing pulse, the response of a spin-1/2 system and a spin-5/2 system with no quadrupolar coupling was investigated. The latter case was studied using aqueous $Al(H_2O)_6^{3+}$. When the flip angles of the pulses making up the composite pulse were carefully adjusted, an echo was observed that was only $1/300^{th}$ the initial amplitude of the free induction decay after the preparation pulse. However, when the flip angles of the pulses were varied significantly from 90° or 180°, the amplitude of this echo increased by as much as a factor of three. If a 180°_{z} pulse was applied during the initial free induction decay (instead of after), then the phase of the signal was altered by 180°, which is clearly an expected result. To determine if some of the observed refocusing in the spin-5/2 solid samples might be the result of a multiple quantum process, the 180°_{z} pulse was applied to the strongly coupled protons in adamantane. Regardless of the accuracy of adjustment of flip angles in the composite pulse, no echo was seen from adamantane.

The existence of an echo after a composite 180°_{z} pulse is now well established. Contrary to the initial interpretation, the echo does not necessarily represent refocusing of the second order quadrupolar interaction, but may originate in the refocusing of interactions that have an I_z spin operator dependence. Results indicate that the excitation of satellite transitions needs to be taken into account in any future attempts to analyze the origin of the echo.

REFERENCES

1. Fyfe, C.; Gobbi, G.; Hartman, J.; Klinowski, J.; Thomas, J. J. Phys. Chem. 1982, 86, 1247.

2. Fyfe, C.; Klinowski, J.; Gobbi, G. Angew. Chem. Intl. Ed. 1983, 22, 259.

3. Fyfe, C.; Gobbi, G.; Kennedy, G.; Graham, J.; Ozubko, R.; Murphy, W.; Bothner-By, A.; Dadok, J.; Chesnick, A. Zeolites, 1985, 5, 179.

4. Behrens, H.; Schnabel, B. Physica 1982, 114B, 185.

5. Samoson, A.; Kundla, E.; Lippmaa, E. J. Mag. Reson. 1982, 49, 350.

6. Kundla, E.; Samoson, A.; Lippmaa, E. Chem. Phys. Lett. 1981, 83, 229.

7. Meadows, M.; Smith, K.; Kinsey, R.; Rothgeb, M.; Skarjune, R.; Oldfield, E. Proc. Natl. Acad. Sci. USA 1982, 79, 1351.

8. Oldfield, E.; Kinsey, R.; Montez, B.; Ray, T.; Smith, K. J. Chem. Soc., Chem. Commun. 1982, 254.

9. Oldfield, E.; Schramm, S.; Meadows, M.; Smith, K.; Kinsey, R.; Ackerman, J. J. Am. Chem. Soc. 1982, 104, 920.

10. Burton, D.; Harris, R. J. Chem. Soc., Chem. Commun. 1982, 256.

11. Ganapathy, S.; Schramm, S.; Oldfield, E. J. Chem. Phys. 1982, 77, 4360.

12. Hahn, I. Phys. Rev. 1950, 80, 580.

13. Lowe, I. Bull. Am. Phys. Soc. 1957, 2, 344.

14. Pound, R. Phys. Rev. 1950, 79, 685.

15. Cohen, M.; Reif, F. In "Solid State Physics", Seitz, F.; Turnbull, D., Ed.; Academic Press: New York, 1957; volume 5.

16. Abragam, A. "The Principles of Nuclear Magnetism"; Oxford: London, 1961.

17. Slichter, C. "Principles of Magnetic Resonance"; Harper and Row: New York, 1963.

18. Kanert, O.; Mehring, M. In "NMR: Basic Principles and Progress", Diehl, P.; Fluck, E.; Kosfeld, R., Ed.; Springer-Verlag: New York, 1971; volume 3.

19. Gerstein, B.; Dybowski, C. "Transient Techniques in the NMR of Solids"; Academic Press: New York, 1985.

20. Stauss, G. J. Chem. Phys. 1964, 40, 1988.

21. Carter, G.; Bennett, L.; Kahan, D. "Metallic Shifts in NMR"; Pergamon Press: New York, 1977.

22. France, P. J. Magn. Reson. 1980, 40, 311.

23. Baugher, J.; Taylor, P.; Oja, T.; Bray, P. J. Chem. Phys. 1969, 50, 4914.

24. Schmidt, V. "Proceedings", 2nd Ampere International Summer School on Pulsed Magnetic and Optical Resonance, Basko Polje, Yugoslavia, 1971.

25. Fenzke, D.; Freude, D.; Frohlich, T.; Haase, J. Chem. Phys. Lett. 1984, 111, 171.

26. Samoson, A.; Lippmaa, E. Chem. Phys. Lett. 1983, 100, 205.

27. Samoson, A.; Lippmaa, E. Phys. Rev. B 1983, 28, 6567.

28. Trokiner, A.; Man, P.; Thevineau, H.; Papon, P. Solid State Commun. 1985, 55, 929.

29. Man, P.; Theveneau, H.; Papon, P. J. Magn. Reson. 1985, 64, 271.

30. P.-J. Chu, Department of Chemistry, Iowa State University, Ames, Iowa, personal communication.

31. Solomon, I. Phys. Rev. 1958, 110, 61.

32. Bonera, G.; Galimberti, M. Solid State Commun. 1966, 4, 589.

33. Weisman, I.; Bennett, L. Phys. Rev. 1969, 181, 1341.

34. Davis, J.; Jeffrey, K.; Bloom, M.; Valic, M.; Higgs, T. Chem. Phys. Lett. 1976, 42, 390.

35. Bloom, M.; Davis, J.; Valic, M. Can. J. Phys. 1980, 58, 1510.

36. Butterworth, J. Proc. Phys. Soc. 1965, 86, 297.

37. Dowley, M. Solid State Commun. 1965, 3, 351.

38. Dowley, M. Phys. Lett. 1967, 24A, 428.

39. Abe, H.; Yasuoka, H.; Hirai, A. J. Phys. Soc. Japan 1966, 21, 77.

40. Flett, A.; Richards, J. Proc. Phys. Soc. 1965, 86, 171.

41. Mansfield, P. Phys. Rev. 1965, 137, A961.

42. Gerstein, B. Phil. Trans. Roy. Soc. A 1981, 299, 521.

43. Freeman, R.; Frenkiel, T.; Leavitt, M. J. Magn. Reson. 1981, 44, 409.

44. Walker, R.; Gerstein, B. Phys. Rev. B 1985, 31, 3167.

SUMMARY

The application of ^{51}V and ^{31}P NMR and EPR to the study of vanadium-phosphorous-oxygen catalysts disclosed the presence of V(III) as well as the expected V(IV) and V(V) in many of the different catalysts examined. The nature of NMR in paramagnetic materials, however, limited the amount of information that could be obtained about the structure of the catalyst. The use of a multiple pulse sequence for the removal of line broadening in the ^{27}Al NMR spectra of zeolites was found to be too complicated to be immediately successful, and the possible origin of an echo was discussed.

ACKNOWLEDGEMENTS

Among those who contributed to the completion of this work, I would particularly like to thank Tom Moser, Bob Wenig, Po-Jen Chu, Serge Lacelle, Joe Iwamiya and Dr. Bernard Gerstein.

I am also grateful to the following: Linda Pearce and Dick Schoenberger for their assistance with EPR, Jim Benson for X-ray work on V_2O_5, and Dr. Ken Windom for providing aluminosilicate samples.